

Instituto Tecnológico y de Estudios Superiores de Monterrey

Campus Monterrey

School of Engineering and Sciences



“Evaluation of the dimensional capabilities for the technologies of selective laser melting and digital light processing, to fabricate micro-cavities: microneedle insert as case of study”

A dissertation presented by

Cindy Paola Meneses Ricaurte

Submitted to the
School of Engineering and Sciences
in partial fulfillment of the requirements for the degree of

Master of Science

Major in Manufacturing Systems

Monterrey Nuevo León, June 16th, 2020

Instituto Tecnológico y de Estudios Superiores de Monterrey

Campus Monterrey

School of Engineering and Sciences

The committee members, hereby, certify that have read the thesis presented by Cindy Paola Meneses Ricaurte and that it is fully adequate in scope and quality as a partial requirement for the degree of Master of Science, with a major in Manufacturing Systems,

Dra. Elisa Virginia Vázquez Lepe
Tecnológico de Monterrey
School of Engineering and Sciences
Principal Advisor

Dra. Erika García López
Tecnológico de Monterrey
Co-advisor

Dr. Ciro Angel Rodríguez González
Tecnológico de Monterrey
Committee Member

Dr. Jesús Alejandro Sandoval Robles
Tecnológico de Monterrey
Committee Member

Dr. Rubén Morales Menéndez
Dean of Graduate Studies
School of Engineering and Sciences
Monterrey Nuevo León, June 16th, 2020

Declaration of Authorship

I, Cindy Paola Meneses Ricaurte, declare that this dissertation titled, “Evaluation of the dimensional capabilities for the technologies of selective laser melting and digital light processing, to fabricate micro-cavities: microneedle insert as case of study” and the work presented in it are my own. I confirm that:

- This work was done wholly or mainly while in candidature for a research degree at this University.
- Where any part of this thesis has previously been submitted for a degree or any other qualification at this University or any other institution, this has been clearly stated.
- Where I have consulted the published work of others, this is always clearly attributed.
- Where I have quoted from the work of others, the source is always given. With the exception of such quotations, this thesis is entirely my own work.
- I have acknowledged all main sources of help.
- Where the thesis is based on work done by myself jointly with others, I have made clear exactly what was done by others and what I have contributed myself.

Cindy Paola Meneses Ricaurte
Monterrey Nuevo León, June 16th, 2020

@2020 by Cindy Paola Meneses Ricaurte
All rights reserved

Dedication

To God, my parents and my family who always believed in me and supported me through my master's degree.

To my friends, who were away but close in the process.

To Jared, for always encouraging me to perform and for giving me his unconditional love.

Acknowledgements

I am deeply grateful for the support of the Advanced Manufacturing Research group here in ITESM, for the support of my advisor Elisa Vázquez and my co-advisor, Erika García whom brought guide and orientation in this long way.

I want to thank to Ulisses Heredia, Erick Ramírez, and Jesús Sandoval, that were people that supported me in the acquisition of knowledge and understanding of the technologies studied in this research.

Finally, I want to thank for my sponsors, the Tecnológico de Monterrey and CONACYT, for giving me the opportunity to study in this great university.

“Evaluation of the dimensional capabilities for the technologies of selective laser melting and digital light processing, to fabricate micro-cavities: microneedle insert as case of study”

By

Cindy Paola Meneses Ricaurte

Abstract

Additive manufacturing technologies are nowadays a feasible resource in micro parts fabrication, which have a wide range of applications from medical industry to injection molding. These technologies allow fabrication of complex parts with a variety of geometries and sizes that ultimately gives a competitive advantage by letting the manufacturing of insert molds.

This research study the dimensional capabilities of selective laser melting and digital light processing to produce microneedle cavities from 500 μm to 2500 μm . An insert for microneedle was manufactured varying its bases geometries and successfully fabricated through selective laser melting at 0°, 45° and 90° orientations. Similarly, for the digital light processing technology, inserts for microneedle geometries were manufactured at 0° and 45° build surface orientation. It was found for the hexagonal base geometry, the best for both technologies with the lower dimensional errors, due to a common factor between processes called stair stepping.

By using a reduction in border and contour power, height dimensional accuracy of the microneedle insert was improved. There was a minimum error of 3% for 600 μm of nominal height corresponding to the fabricated insert by selective laser melting at 0° orientation of construction with the optimal design.

List of figures

Figure 1. Representation of the digital light processing technology. Source [6]	8
Figure 2. Representation of the selective laser melting process	10
Figure 3. Phase 1 of the research	16
Figure 4. Phase 2 of the research	17
Figure 5. Top view for positive and negative construction	17
Figure 6. Lateral view test sample for positive construction	18
Figure 7. Lateral view test sample for negative construction	18
Figure 8. Microneedle insert, top view	19
Figure 9. Microneedle insert, lateral view	19
Figure 10. Configuration for initial samples in QuantAM software	22
Figure 11. Representation of borders and fill contours in negative (left) and positive (right) microneedles construction	22
Figure 12. Inserts building orientation. A) 0° B) 90 °and 45° in QuantAM. Software	24
Figure 13. Layer configuration for microneedles at 0° of build surface orientation (A) and border and contours representation in conical base (b).....	25
Figure 14. Layers configuration for microneedles at 90°	26
Figure 15. Inserts build surface orientations. A) 0° B) 45° in digital light processing	26
Figure 16. Representation of variable for a) positive and b) negative constructions	27
Figure 17. Height measurements representation for bases a) conical, b) triangular, c) square, d) pentagonal and e) hexagonal	28
Figure 18. Side lengths measurements representation for bases a) conical, b) square, c) hexagonal, d) pentagonal and d) triangular	29
Figure 19. Tip radius measurement.....	29
Figure 20. Top side measurement for runner	30
Figure 21. Lateral side measurements for runner.....	30
Figure 22. Microneedle height for positive and negative constructions in SLM	31
Figure 23. Side results for positive and negative constructions in SLM.....	32
Figure 24. Corners configuration for negative microneedles square sides a) QuantAM software and b) Ideal square geometry	33
Figure 25. Relative error for height variable	34
Figure 26. Relative error for side variable.....	35
Figure 27. Tip radius for positive microneedles in selective laser melting	36
Figure 28. Lateral view in microscope for heights: from 1000 μm to 2500 μm for bases conical (A-D), triangular (E-H), square (J-M), hexagonal (N-P)	37
Figure 29. Height results for negative construction in digital light processing	38
Figure 30. Sides results for negative construction in digital light processing.....	39
Figure 31. Capabilities for height variable in negative construction for SLM technology	40
Figure 32. Capabilities for height variable in negative construction for DLP technology	41
Figure 33. Stair stepping effect for layer thickness l and building angle α. Retrieved from [55]	42

Figure 34. Angle for lateral microneedle cavity.....	43
Figure 35. Height results for microneedle insert.....	44
Figure 36. Top View for microneedles bases in 0° build surface orientation A) conical, B) triangular, C) square, D) pentagonal, E) Hexagonal.....	45
Figure 37. Side variable for Microneedle insert.....	46
Figure 38. Hexagonal base geometry construction at A) 0°, b) 45° and C) 90°.....	46
Figure 39. Top surface roughness average value.....	47
Figure 40. Surface topography for build surface orientations. A)0° B)45° C)90° ...	48
Figure 41. Microneedles inserts from left to right at 0°,45° and 90°.....	48
Figure 42. Parameters comparison for height variable in build surface orientation 0°.....	49
Figure 43. Parameters comparison for height variable in build surface orientation 45°.....	50
Figure 44. Parameters comparison for height variable in in build surface orientation 90°.....	50
Figure 45. Dross formation effect at 90° build surface orientation.....	52
Figure 46. Comparison for this research in literature for negative microneedle construction with VAT photopolymerization technology.....	55
Figure 47. Comparison for this research in literature for negative microneedle construction with SLM technology.....	56
Figure 48. Build surface orientation for positive and negative microneedles.....	60
Figure 49. Distribution of test pieces in the base plate.....	60
Figure 50. 0° build surface orientation for microneedle insert fabrication.....	61
Figure 51. 90° of build surface orientation for microneedle insert fabrication.....	61
Figure 52. 45° build surface orientation with offset.....	62
Figure 53. Microneedle insert at 45° build surface orientation with supports.....	62
Figure 54. Distribution in base plate for 0°,45° and 90° build surface orientations	62
Figure 55. Electropolishing diagram.....	63
Figure 56. Electropolishing results for insert at 0° build surface orientation.....	64
Figure 57. Ultrasonic injected Microneedle pieces. From left to right SLM insert, SLM insert and DLP insert.....	68
Figure 58. Height results for Microneedles in ultrasonic injection molding process	69
Figure 59. Side results for Microneedles in ultrasonic injection molding process..	69
Figure 60. Tip Radius for Microneedles with ultrasonic injection Molding.....	70
Figure 61. Height relative error for negative construction in SLM.....	71
Figure 62. Height relative error for positive construction in SLM.....	72
Figure 63. Side relative error for negative construction in SLM.....	72
Figure 64. Side relative error for positive construction in SLM.....	73
Figure 65. Height relative error for negative construction in DLP.....	73
Figure 66. Side relative error for negative construction in DLP.....	74

List of tables

Table 1. Literature review	14
Table 2. SS 316L-0407 powder chemical composition.....	20
Table 3. SS 316L-0407 powder characteristics	20
Table 4. HTM 140. Materials properties	21
Table 5. Phase 1 parameters	23
Table 6. Border and fill contour parameters	23
Table 7. Phase 2 parameters	24
Table 8. DLP parameters	27
Table 9. Alicona parameters.....	29
Table 10. Angles for different geometries.....	43
Table 11. Dimensional measurement for microneedle inserts.....	53
Table 12. Runner and gate measurements for SLM.....	54
Table 13. Abbreviations.....	59
Table 14. Acronyms	59
Table 15. Electropolishing process parameters.....	63
Table 16. Process parameter for UIM samples	65
Table 17. Top view for injected microneedles	66
Table 18. Hypothesis test for triangular base at 0° orientation	75
Table 19. Hypothesis test for conical base at 0° orientation.....	75
Table 20. Hypothesis test for square base at 0° orientation	76
Table 21. Hypothesis test for pentagonal base at 0° orientation	76
Table 22. Hypothesis test for hexagonal base at 0° orientation.....	76
Table 23. Hypothesis test for triangular base at 45° orientation	77
Table 24. Hypothesis test for conical base at 45° orientation	77
Table 25. Hypothesis test for square base at 45° orientation	77
Table 26. Hypothesis test for pentagonal base at 45° orientation	78
Table 27. Hypothesis test for hexagonal base at 45° orientation.....	78
Table 28. Hypothesis test for triangular base at 90° orientation	78
Table 29. Hypothesis test for conical base at 90° orientation.....	79
Table 30. Hypothesis test for square base at 90° orientation	79
Table 31. Hypothesis test for pentagonal base at 90° orientation	79
Table 32. Hypothesis test for hexagonal base at 90° orientation.....	80

Table of contents

Abstract	vii
List of figures	viii
List of tables	x
Chapter 1.....	1
1. Introduction.....	1
1.1 Motivation.....	2
1.2 Problem Statement	2
1.3 General Objective	3
1.4 Specific Objectives.....	3
Chapter 2.....	4
2. Background.....	4
2.1 Microneedles.....	4
2.1.1 Microneedle manufacturing.....	4
2.2 Additive manufacturing technology in microneedle production.....	7
2.2.1 Positive microneedles manufactured with additive manufacturing	9
2.2.2 Master mold microneedles manufactured with additive	
manufacturing technologies.	12
Chapter 3.....	16
3. Methodology	16
3.1 Design of test samples and Microneedle insert.....	17
3.2 Materials.....	19
3.2.1 Selective laser melting process (SLM)	19
3.2.2 Digital light processing (DLP)	20
3.3 Equipment	21
3.3.1 Selective laser melting	21
3.3.1.1 Parameters.....	21
3.3.1.2 Parameters modification.....	25
3.3.2 Digital light processing	26
3.3.3 Characterization	27
Chapter 4.....	31
4. Results and discussion	31
4.1 Phase 1 Results	31

4.1.1	SLM: Microneedles bases characterization for positive and negative constructions.....	31
4.1.2	Optical characterization of microneedles in positive construction	37
4.1.3	Digital light processing: Microneedles bases characterization for negative construction	38
4.1.4	Selective laser melting and digital light processing height relative errors	40
4.2	Phase 2 Results: Insert manufacturing with selective laser melting and digital light processing.....	43
4.3	Results for Microneedle insert measurements	53
4.4	Results validation	55
Chapter 5	57
Conclusions	57
Appendix A: Abbreviations and acronyms.....		59
Appendix B: QuantAM preparation.....		59
Appendix C: Preliminary electropolishing studies.....		63
Appendix D: Preliminary samples in ultrasonic injection process		65
Appendix E: Relative error graphs.....		71
Appendix F: Hypothesis tests results		75
Bibliography.....		81
Curriculum.....		87

Chapter 1

1. Introduction

Medical devices obtained from an additively manufactured process are becoming a trend year by year. Globally, its use has increased in statistics; thus, has led to a growth in the market share, although there are little regulations about this subject (ISO 13485), more researchers are interested in exploring more about it [1]. Specifically, the industry of the drug delivery system would be one of the most promising markets by 2026. It is projected to reach values of USD 1,790.6 billion by the end of that year. These areas are the main target for this research, main topics are based on a proposal, design and fabrication of a microneedle insert with additive manufacturing that could be used in the ultrasonic injection molding process [2].

Nowadays, microneedle manufacturing can be constructed with the positive, which means that the microneedle will be fabricated directly with the final form to be used, or the negative feature of the microneedle using a mold or insert cavity [3]. Some of the most common techniques for positive production are etching, machining, lithography and laser cutting. On the other hand, to produce the negative shape insert, there are technologies like electrical discharge machining, micro milling, laser beam machining [4]. This research is focus on the negative form of the microneedle manufacturing as molds and cavities fabrications.

The design of cavities for molding and master molds have been fabricating with conventional process as mentioned. However, the additive manufacturing technology started its first investigations last years. Authors like Krieger, Lacan and Boehm [5][6][7] have been conducting studies about processes of stereolithography and digital light processing to produce molds for microneedles. For digital light processing by laser, one DLP chip projects an image on a photosensitive resin. Then, the resin is cured and solidified by the source light. The difference between each process is that for stereolithography, the laser draws in the x and y plane and

in the digital light processing the lens projects the cross-sectional section of a 3D sample [8].

Selective Laser Melting is another additive manufacturing technique, which comprehend the study in this research. This process is able to fabricate 3D models through a layer system where initially, a powder layer is deposited on a base plate, and then selectively the laser scans the desired geometry, followed by a roller movement whose function is to drop a new powder layer and scan the new slice. In this way, the layers bound continuously until finishing the 3D model [9]. This technique has only been studied by Gieseke with Microneedle application in the positive form [10]. Vazco and Pouzada also used the same selective laser melting technique to produce micro tool inserts to be use in the process of injection molding [11]. In an alternative study, they explain the viability of the use of selective laser melting process to fabricate inserts or micro tools to be applied in thermoplastics molding [4].

1.1 Motivation

Fabrication of a mold with micro features is expensive with the conventional manufacturing processes because it involves the fabrication of many components with great precision. Actually, additive manufacturing is becoming an excellent choice to produce final parts with great accuracy with advantages as complexity of the design and variation of sizes. An insert application leads to a product personalization and reduction of costs for injection molding industries.

1.2 Problem Statement

Additive manufacturing technologies as selective laser melting, and digital light processing have not been studied for fabrication of microneedles inserts. Although both technologies have been tested to produce the positive form of the disposable microneedles, there are no previous investigations towards this application in negative or cavities for microneedles.

1.3 General Objective

To study dimensional capabilities for technologies of selective laser melting and digital light processing for the fabrication of mould insert for microneedles geometries.

1.4 Specific Objectives

- To fabricate different base geometries for microneedles cavities varying height and side between 500 - 2500 μm .
- To analyze different fabricated geometries for microneedles through dimensional characterization, in order to establish an optimal design.
- To study the dimensional capability for the technology of selective laser melting in the fabrication of positive microneedles.
- To fabricate a microneedle insert with technologies of SLM and DLP.
- To study different surface build orientation angles, for the manufacturing of the microneedle inserts.

1.5 Main contributions

- This work is a starting point to produce molds for micro sizes in technologies of selective laser melting and digital light processing that could be applied in ultrasonic injection molding technology.
- Selection of an optimal base design that can be used for future insert molds fabrication.
- Study of different geometries to improve height accuracy in microcavities for layer-based system fabrication technologies.
- Determine a range of capabilities in terms of dimensional errors for microcavities in selective laser melting and digital light processing.
- Study of parameters for microcavities with inclination angle.
- Determine a specific border and contour power that improved the z resolution of microneedle cavities.

Chapter 2

2. Background

2.1 Microneedles

Microneedles are a painless device due to its small size; meaning that it does not induct pain in the human body because it reduces the stimulation on nerves [12]. These devices allow transfer signals or a substance into the skin [5].

Microneedles have a wide range of materials, sizes, and geometries; about the sizes there are in the micron range, which can vary length from 50 to 900 μm [13]. Although, some researchers have carried out investigations with higher lengths up to 3000 μm in order to get information about the manufacturing capabilities [5]. In geometries, there have been studied square, circular, flat tipped, sharp tipped, hollow, pyramidal, and conical [10] [14] [15]. Honeybee stinger also was a bio design applied on microneedles, which were manufactured by a magnetorheological drawing lithography method. The research concluded that this type of geometry is favorable because of easy insertion and removal in the skin due to lower friction forces in the design [16]. Implying materials such as metals, silicon, polymers, ceramics, silica glass, carbohydrates; there are many options with advantages and disadvantages on the manufacturing for microneedles. The selection would be according to the product final application (drug delivery, patient monitoring, cosmetic applications); that is why it is important to consider its strength, young modulus, toughness, biocompatibility, and biodegradability [13].

2.1.1 Microneedle manufacturing

Microneedles can be fabricated by direct application, which means that will be manufactured the positive geometry of the microstructure; or by using a master mold. This master mold is the negative shape of the desired microneedles [3].

Several cases have been studied with direct manufacturing techniques as the case of metal microneedle, which are fabricated by electroplating, photochemical

etching, laser cutting and surface micro milling [17]. There are some others as lithography, micro-drilling, and casting. In the master mold technique, some of the ones use are casting, hot embossing, injection molding [18].

In order to get an array to compile microneedles, there is necessary a master mold or cavity with the negative shape [3]. There have been technologies studied in manufacturing to produce negative molds with micro range capabilities:

Electric discharge machining (EDM). It is a nontraditional process where thermal energy is used in a removal process with high precision by generating a spark with the sample. There is no contact between the part and the electrode. The erosion is constant and is controlled by the electric spark which is created in a dielectric liquid. This liquid is located between the workpiece and the electrode. This method has been used in the production of die cavity for high precision parts [19].

Micro milling. This has been studied for the creation of steel mold inserts for micro features manufacturing. Fully hardened steel has been machined with tools of 50 μm diameter. The production time depends on the complexity of the design, meaning that the technique can be expensive for micro molding applications [3].

After fabricated the negative molds, there are a variety of process to finally produce parts in large quantities:

Hot embossing. It is a process divided in 4 stages according to Becker and Heim: the idea, master, replication, and completion. After the idea has been defined, a master is fabricated with photolithography. Then it is mounted in the embossing machine. The embossing tool: made commonly of nickel or silicon, and the polymer substrate are mounted on the heating plate. In this area, there are cooling channels, that properly configured allow stabilization of temperature between the tool and the polymer substrate. When the cycle starts, both elements are heated separately in a chamber with a vacuum above the glass at polymer transition temperature. Finally, after reaching the lowest temperature, the embossing tool is removed by a mechanical action [20].

Microinjection molding. It is an efficient and low-cost manufacturing technique that produces a large number of microneedles simultaneously. That is why it's applicable for mass production systems [21]. There are different methods for cavities manufacturing and the accurate selection for each one depends on the desirable final surface quality. Studies had concluded that high melts, high mold temperatures, and high injection speed are suitable for filling microcavities [22].

Ultrasonic injection molding (UIM). This technology uses a vibration energy to melt the polymeric material that can fabricate microparts just as the process of micro injection molding. According to Dorf et al., there are 3 important phases: dosing, melting, and cooling. Firstly, the polymer material or feedstock in pellets' form is put into the chamber, then the plunger moves toward the vibrating sonotrode compressing the polymer and by thermal energy, the polymer melts and fill the cavity, after the part is solidified and ejected [23].

Heredia et al describes the potential application of this technology for microneedles production and recognizes as a promising technique for micro scale fabrication in a short time cycle with bigger amount of savings in energy [24].

Gulcur et al. manufactured a microneedle insert with a machining process to be used in an ultrasonic microinjection molding machine (Sonorus 1G Ultrason). A nano fingerprint with an optical gadget was included into the device for quality inspection of microneedles. Results of one injection sample exhibited a height of 510 μm a tip radius of 40 μm . These authors also led another research [25] using microinjection molding with a microneedle insert. In this case, the researchers used a thermal visualization system to control the maximum temperature distribution. The insert cavity had conical microneedles of 600 μm of height and 300 μm of diameter. Thicknesses of the polypropylene pellets discs were studied, and results suggest that, with the lower thickness of 0.5 mm the system reached the maximum temperature, that results in better melting. However, in the height parameter this thickness was not the best as the 1mm thickness with a height of 455 μm . This was the highest value for a 1 mm thickness. The lowest recorded was 410 μm .

2.2 Additive manufacturing technology in microneedle production

A new group of technologies are becoming popular in the manufacturing of medical and biomedical devices, especially in microneedles; that group is additive manufacturing (AM) with continuous increasing in usage because AM is cost effective and it's possible to create personalized prototypes with complex structures [26]. This technology is based initially in the design of a 3D object through a software. Then, the model usually will build layer over layer [27]. This technology can be used to produce positive or negative geometries according to the reference literature.

According to the ISO/ASTM 52900:2015 [28] there are seven groups of additive manufacturing technology; binder jetting, directed energy deposition, material extrusion, material jetting, powder bed fusion, sheet lamination and vat photopolymerization. Not all the groups have been explored in the production of microneedles because of its capabilities and low material range availability. Photopolymerization is one of the most used to microneedles fabrication.

Projection based direct light processing (DLP). This technology has been applied in the microneedles manufacturing constitutes the group of photopolymerization as previously mentioned. It includes a projector where cross sectional parts of an object are flashed at once by pixels. As long as the layer has been finished, the platform moves down if the UV light source is above the platform or moves up when the UV light source is below. The following step involves the previous layer, which has uncured resin. It is exposed to the light to be solidified. This will repeat until finishing the 3D shape completely [8] [5]. The main component of this technology is a digital micromirror device that was developed by Texas instruments. The chip is formed by many tiny mirrors, which have two directions movements. Its configuration allows to build a part in voxels instead of layers [29].

Figure 1 is a schematic representation of the system in a digital light processing process. This is configured by a build platform, the photopolymer, a transparent base, lens, light source, and finally the digital light processing process.

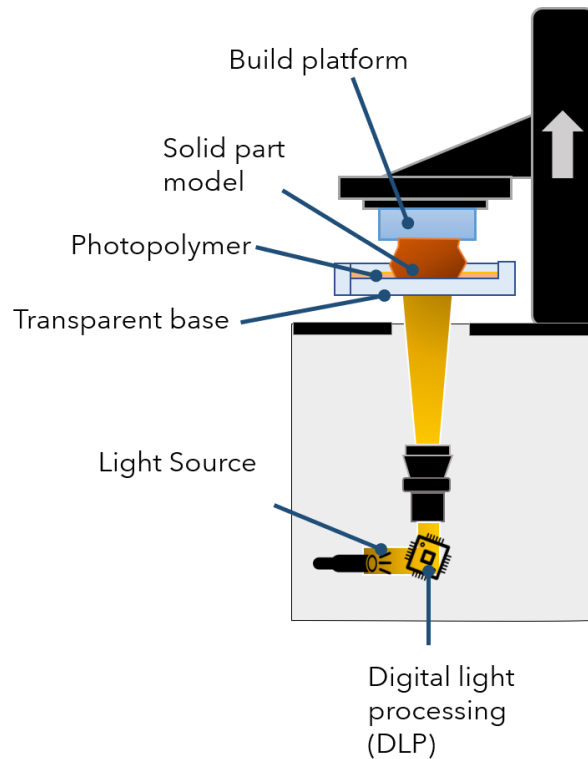


Figure 1. Representation of the digital light processing technology. Source [6]

Stereolithography (SLA). This technique is part of the photopolymerization group additive manufacturing. It is similar to DLP technology due to the use of a photosensitive resin that will be cured. Despite of the principle, the differences lies on it has a laser (instead of a projector) which draws each layer across X and Y axis [8].

Selective laser melting (SLM). This manufacturing method is included in the powder bed fusion group of additive manufacturing technologies, which uses a laser as a power source. Based on a STL 3D design, the laser selectively melts the metal powder based on the desired slices. Once a layer has been scanned, the platform moves down according to the settle layer thickness and another powder bed is applied on the top of the built layer. The process will continue to melt powders and bond layers until the STL model has finished [30]. Figure 2 shows a representation of the technology.

One experiment was carried out by Vazco and Pouzada to manufacture with the SLM process a logo insert with 100 μm of width and a height of 300 μm . The machine was a sintering equipment EOSINT M270 (EOS Germany). The study used as material, a stainless-steel powder with an average grain size of 30 μm and the selected thickness layer was 20 μm . The research concluded that it was necessary to do a post process step because the horizontal and lateral roughness were not appropriate to get microfeatures in the ultrasonic injection molding process. Also, the study determined that the measured widths were longer than the 3D CAD specifications [11].

2.2.1 Positive microneedles manufactured with additive manufacturing

Hollow microneedles with size between 80 μm and 320 μm were manufactured with a positive construction, using the process of micro selective laser melting; followed by a femtosecond laser to drill the Microneedles. The material selected was a stainless-steel alloy 316 L and the ground conditions were 21 W laser power and 225 mm/s scan speed. The results showed microneedles with a height of 1200 μm with an inner diameter of 120 μm and outer diameter of 200 μm . The post processing methods were applied ultrasonic cleaning and plasma polishing. However, those did not successfully remove the adhesion of the particles [10].

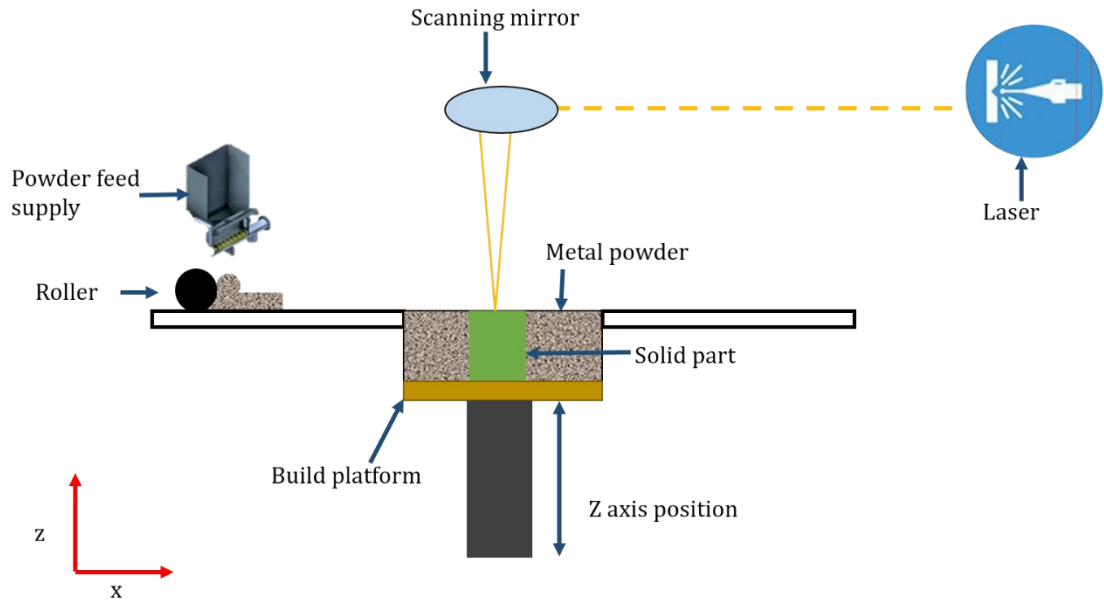


Figure 2. Representation of the selective laser melting process

Two photon polymerization process (2PP) was applied to manufacture positive solid microneedles with the following set of parameters for the system: a laser of 8-12 mW of power, layer spacing of 10 μm , raster spacing of 5 μm , and a scanning speed of 200 $\mu\text{m/s}$. The author in this investigation was able to manufacture 4 microneedles at the same time [31].

Stereolithography is another manufacturing technique, which has been investigated for positive microneedle's production. Pere et al. [26] used this method to manufacture pyramidal and conical microneedles of 1 mm of height and base; an interspacing distance of 1.85 mm. This study manufactured patches of 48 microneedles using a Form 2 stereolithography printer by Form labs with a biocompatible resin. Later, the microneedles were coated with insulin with the inject printing method. The research made a comparison of the insertion forces on porcine skin. Between conical and pyramidal designs, the results exposed that cone design required less force to penetrate than pyramidal. A difference of 21% on insertion force is coherent due to the frictional forces on the pyramidal design were greater than the cone because of the lateral area of contact with the skin leading to greater loads.

Stereolithography manufacturing technique was used by Farias et al. [32] to produce an array of 13 conical microneedles with nominal dimensions with a diameter of 1000 μm , height of 600 μm and tip radius of 162.5 μm for the application of microencapsulated cell extrusion. Form labs 2 machine was used, the results about the tip radius were 160 $\mu\text{m} \pm 20 \mu\text{m}$ and the root mean square roughness gotten for the microneedle was 158 nm.

Johnson and Procopio [33] studied another additive manufacturing technique for microneedles s production Through digital light processing, a square pyramidal array of 144 Microneedles was manufactured with heights of 1000 μm and widths of 450 μm . An Autodesk print studio software was used with 3 nominal layer thickness of 50 μm , 25 μm and 10 μm . The best result corresponding height value was gotten with the lower layer thickness of 10 μm . However, it is noticeable a reduction of 30% in height compared to the nominal. Results exposed that increasing the height maximizes the standard deviation. On the other side, the output width values were near to the nominal value. The tip radius results were at the range of 40-160 μm . It is important to mention that the highest tip radius was obtained with layer thickness of 50 μm . After executed, the algorithm found a minimum error of 5% in height.

Gittard et al. [34] studied the DLP process in the manufacturing of microneedles with the addition of antimicrobial coatings of silver and zinc. The research used a Perfactory III SXGA+ system printer to produce conical and pyramidal microneedle, with heights of 1000 and 1250 μm for each design and widths of 500 and 750 μm . Their results exposed shorter heights in the conical design with a relative error of 17.5%. In contrast, the pyramidal exhibit a bigger error of 33.5% in the height of 1000 μm . In addition, widths were larger than the input value because of the lateral voxel size. However, the dimensional error for width is lower than height variable. When the width increased, so the dimensional error; with a maximum of 8.9% for 750 μm .

Miller et al. [35] used the integration of carbon fiber electrodes as an application in microneedles to be implemented as an electrochemical biosensor. The design of the microneedle was hollow with a tetrahedron base. This device was

manufactured based on the digital light processing technology (Perfactory III SXGA+ instrument) with heights and side lengths of 1.5 mm and 1.2 mm, respectively. After the manufacturing process, the device had heights of approximately 1030 μm with a relative error of 0.31. Whereas the side length was 1120 μm with a relative error of 0.06. Thus, supporting past investigations where was common to find that the side lengths had a better accuracy in this process than height output values.

2.2.2 Master mold microneedles manufactured with additive manufacturing technologies.

Lacan et al. [6], fabricated with digital light processing a microneedle insert, with a conical design and height of 900 μm . Microneedles were drilled with a 355 nm laser wavelength with pulses of 8 pico seconds. The microneedle inserts exhibited height of 886.1 μm . Finally, a penetration test was carried out. However, the authors concluded that it was not able to get the desired sharpness to be used in the injection molding process. The authors suggested to do further investigations to produce final parts with the microneedle insert.

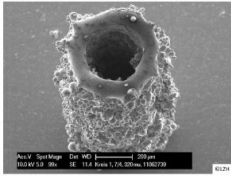
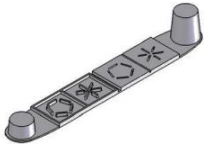
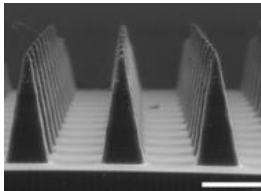
Boehm et al. explored the inject printing and drawing lithography processes for the microneedle molds production, using a Perfactory III Sx GA+ instrument. Firstly, it was manufactured with drawing lithography master mold with an array of 1*5 microneedles. The designs were conical with heights of 500 μm and 1000 μm and base diameter of 500 μm using as resin an e-shell 200 biocompatible acrylate-based polymer. Secondly the master mold was used to fabricate molds of polydimethylsiloxane (PDMS). Thirdly, inject printing technique was used to deposit quantum dot solution. A scanning electron microscopy confirmed final dimensions for microneedles with height of $926 \pm 76 \mu\text{m}$ and base width of $465 \pm 22 \mu\text{m}$ [7]. Another Boehm experimentation was conducted with the same procedure and material with modification in the microneedle base design with height of 1000 μm and side lengths of 500 μm . A triangular base model was tested but the dimensions were lower than conical. Results were height of $833.8 \pm 13.4 \mu\text{m}$ and base width of $381.2 \pm 7 \mu\text{m}$ [36].

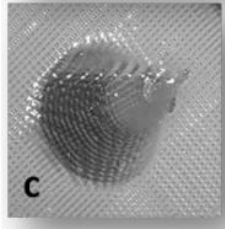
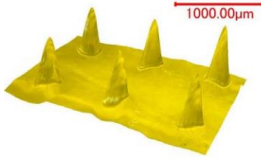
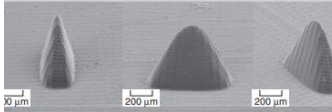
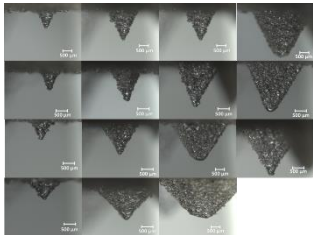
Krieger et al. [5] studied the process of stereolithography in microneedles fabrication. First by developing a 3D printing array and then filling with UV curable resin to obtain a microneedle master. The second stage was to obtain a female mold by silicone casting. This research was focus in the geometric parameters that are important for quality of the process as tip sharpness, height, and aspect ratio. A form 2, form labs SLA 3D printer was used to produce microneedles heights from 0.2 mm to 3 mm with a layer thickness of 25 μm and 3 ratios aspects were tested: 3:1; 4:1 and 5:1. Results suggested that increasing the input height and reducing the aspect ratio, the dimensional error is reduced. About the tip radius, it decreases by decreasing the input needle height.

Qi et al. [21] manufactured microneedles cavities in PDMS using a pattern technique process with a laser. Six patterns were studied: a point array, 2 circles array of 0.04- and 0.06-mm diameter, 2 helix array of 0.08 mm diameter with 3 and 6 turns and last a helix array with 3 turns and 0.1 mm diameter. First, PDMS sheets were created followed by microcavities manufacturing using a laser engraving machine. Finally, the PDMS mold was filled with Polylactic acid (PLA) with temperature of 200 °C. PLA was then cast on the mold. The maximum height exhibited (height of 884 μm and diameter of 350 μm) was obtained with the model of helix array and 6 turns. The lower height corresponded to the circle array of 0.06 mm diameter with 460 μm).

Table 1 is a resume of the principal researchers and authors, which were base for this investigation.

Table 1. Literature review

Reference	Figure	Dimension	Technology	Material	Responses
[10]		Inner diameter 160 μm . Microneedles of size 80 - 320 μm	SL μ M Author machine	Stainless steel alloy 316L, powder	Height, inner diameter, wall thickness
[11]		Heights of 300 μm and widths of 100 μm	SLM: (Eosint M270) SLA: (Viper Si2 3D)	Stainless steel powder, epoxy resin Nano Form 15120	Surface roughness, tool wear, tool integrity.
[33]		Height of 1000 μm and width of 450 μm	DLP: Autodesk® Ember	Autodesk's Standard Clear PR48 Resin	Height, width, tip radius of curvature

Reference	Figure	Dimension	Technology	Material	Responses
[6]		Heights of 300, 600 and 900µm	DLP: (Perfactory® SXGA+ W/ERM Mini Multi Lens)	Acrylate based photopolymer R11	Height, tip diameter
[37]		Height of 990 µm	DLP: Author machine	Poly-ethylene glycol diacrylate (PEGDA)	Height, tip diameter
[34]		Heights of 1000 µm and 1250 µm. Base dimensions of 500 µm × 250 µm and 750 µm × 250µm	DLP: Perfactory III SXGA + system	eShell 200 Envision Tec	Height
Meneses, C		Heights and sides [500, 600, 1000, 1500, 2000, 2500] µm	DLP: Envision Tec SLM: Renishaw AM 400	HTM 140 And stainless-steel powder SS316L	Height, sides, tip radius, surface roughness.

Chapter 3

3. Methodology

This chapter contains all the procedure for this research, shown in Figure 3 and Figure 4. The present investigation is illustrated in 2 stages. The first one was a test around microneedle geometries bases and evaluate the capabilities of the DLP and SLM process with negative geometries for DLP and SLM and positive construction for SLM. The insert was manufactured with both technologies. Each one of these phases contains the dimensional characterization. Initially, the materials and equipment are described to introduce thought the methods used in each phase.

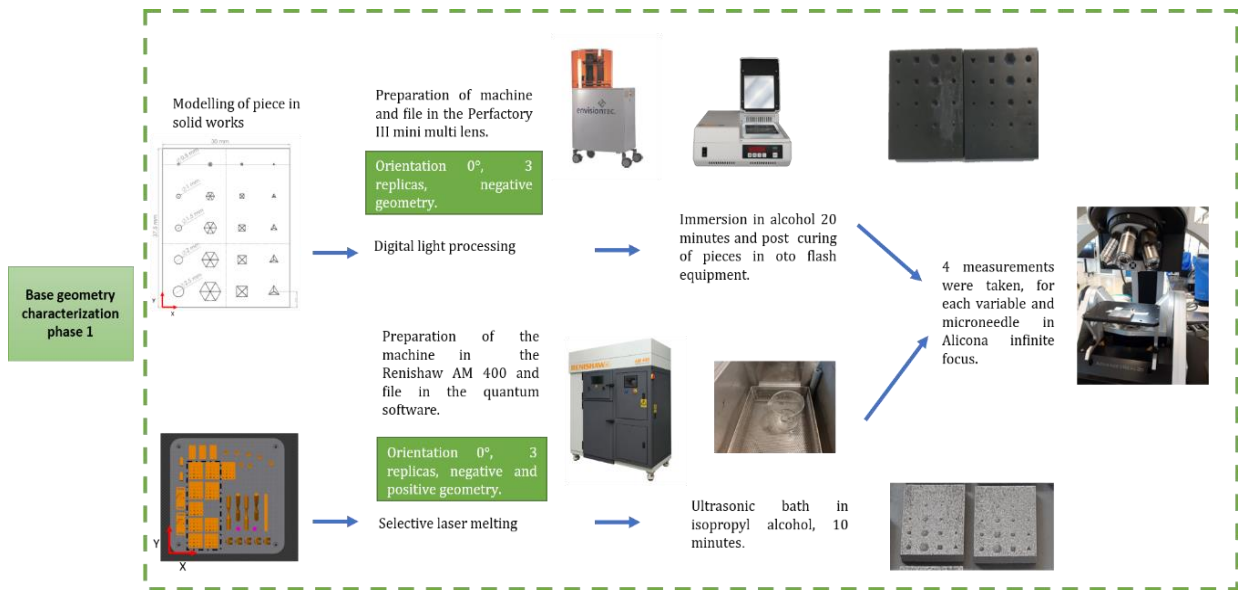


Figure 3. Phase 1 of the research

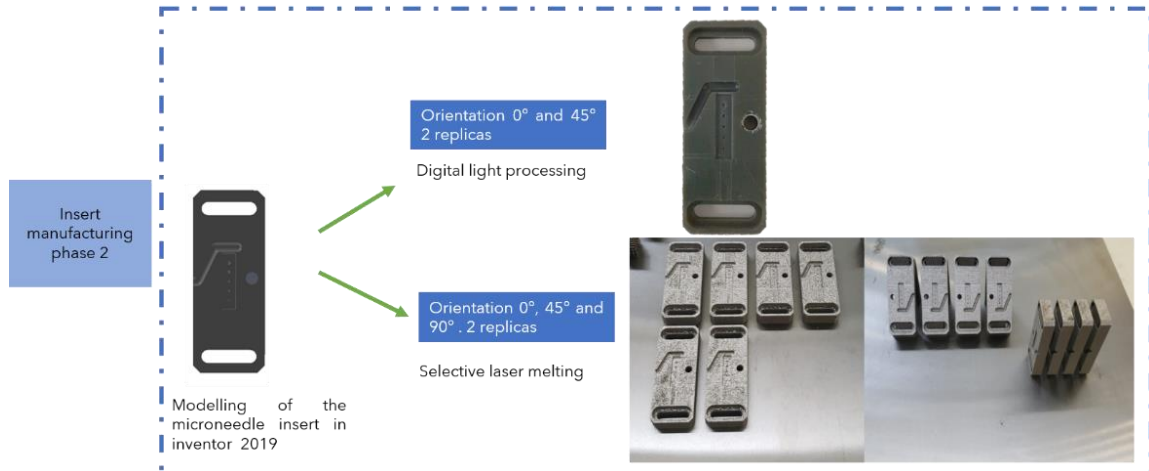


Figure 4. Phase 2 of the research

3.1 Design of test samples and Microneedle insert

Initial sampling for microneedle base characterization was modeled in Solidworks 2018. Two test samples were built with 3 replicates for each one. Top view for positive (sample 1) and negative construction (sample 2) can be observed in Figure 5. Positive construction of microneedles with height of 500 μm , 1000 μm , 1500 μm , 2000 μm and 2500 μm detailed in Figure 6. All microneedles had a ratio aspect of 1:1. The second sample is shown in Figure 7; for negative construction of microneedles.

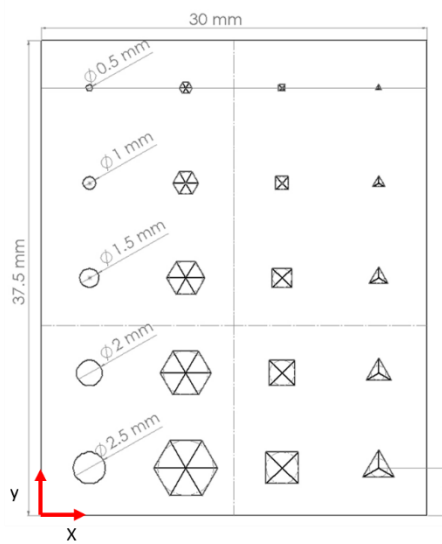


Figure 5. Top view for positive and negative construction

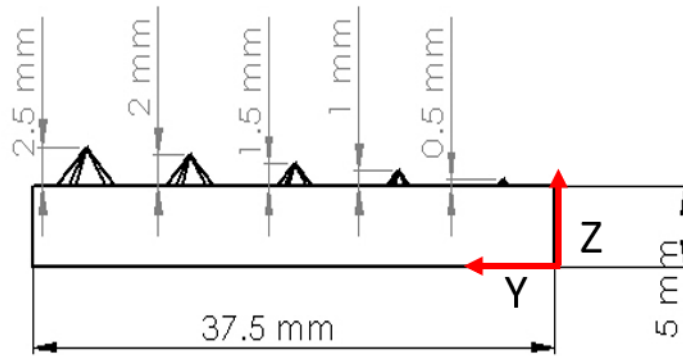


Figure 6. Lateral view test sample for positive construction

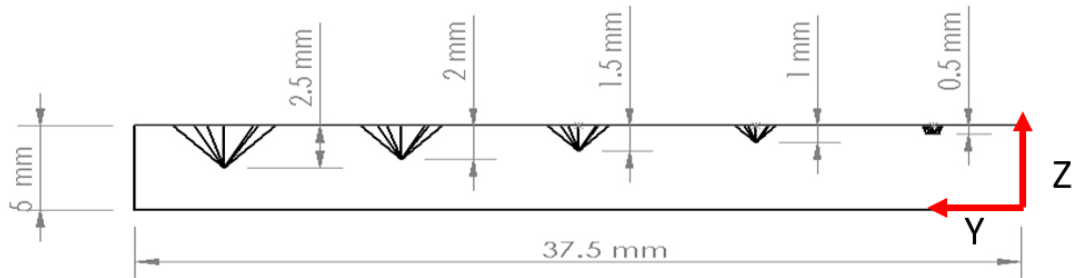


Figure 7. Lateral view test sample for negative construction

Microneedle insert modeling was carried out with Inventor 2019. The insert was composed by a cavity with 5 microneedles of 600 μm height with a ratio aspect of 1:1. The design was composed by 8 cooling channels with 1 mm depth. The runner was designed according to the specifications of the mold cavity 2.38 mm diameter. Top and lateral view of the insert can be observed in Figure 8 and Figure 9. Two replicas were fabricated for each one of the process studied in this research.

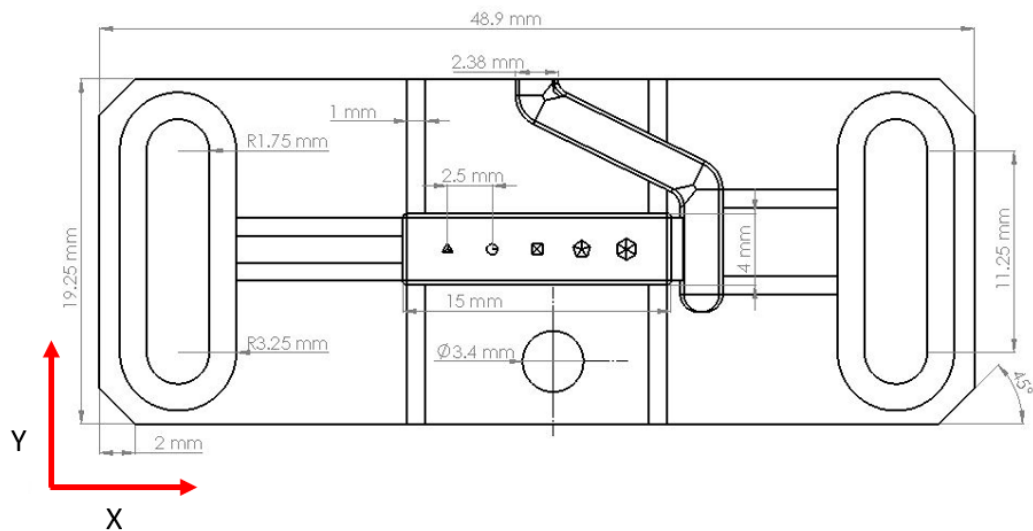


Figure 8. Microneedle insert, top view

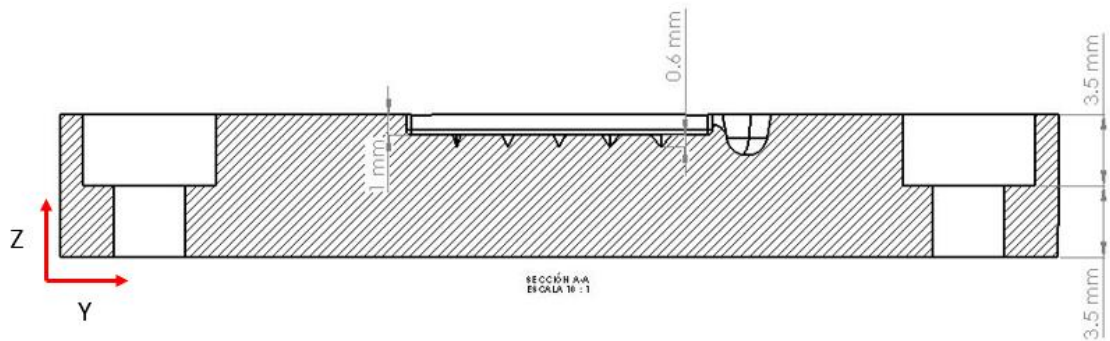


Figure 9. Microneedle insert, lateral view

3.2 Materials

3.2.1 Selective laser melting process (SLM)

The material selected for this study was stainless steel SS 316L-0407 powder provided by Renishaw company. This alloy is an austenitic stainless steel with particle average size of $40 \pm 15 \mu\text{m}$. Chemical composition is detailed in Table 2. This material exhibits good properties as high hardness, toughness, and corrosion resistance. It can also be polished. It was suitable for this research by reason its application in plastic injection [38]. Other characteristics are described in Table 3.

Table 2. SS 316L-0407 powder chemical composition

Element	Mass (%)
Iron	Balance
Chromium	16 -18
Nickel	10 -14
Molybdenum	2 -3
Manganese	≤2,0
Silicon	≤1,0
Nitrogen	≤0,1
Oxygen	≤0,1
Phosphorus	≤0,045
Carbon	≤0,03
Sulphur	≤0,03

Table 3. SS 316L-0407 powder characteristics

Description	Value
Density	7,99 g/ cm ³
Thermal conductivity	16,2 W/mK
Melting range	1371°C – 1399°C
Coefficient of thermal Expansion	16 10 ⁻⁶ k ⁻¹

3.2.2 Digital light processing (DLP)

Resin HTM 140 was purchased from Envision Tec Company. This photosensitive resin is used in procedures that require thermal resistance as the case for ultrasonic injection molding [39]. Table 4 present the meanly materials properties. The photocurable resin had a voxel depth 50 μm, an irradiance value of 700 mW/dm².

Table 4. HTM 140. Materials properties

Description	Value
Tensile strength	56 MPa
Elongation at break	3,5%
Flexural Strength	115 MPa
Flexural Modulus	3350 MPa
Heat deflection temperature	140 °C
Color	Green

3.3 Equipment

3.3.1 Selective laser melting

Renishaw AM 400 was used in this research to produce the microneedle inserts. This machine has 400 Watts of maximum power and a fabric dimensions of 250 mm *250 mm* 300 m. The laser has a wavelength of 1075 nm and a spot laser diameter of 70 µm [40].

3.3.1.1 Parameters

In stage one, the parameters selected are based on Ramirez Cedillo et al research [41]. It was selected a meander scanning strategy at 170 W; contour and border at 170 W; hatch distance of 0.06 mm; point distance of 80 µm, beam compensation of 0.0225 mm; layer thickness of 50 µm; exposure time of 80 µs, two exposures for the top layer and one for the bottom layer, a detailed description of parameters for phase 1 is in Table 5. Finally, a density energy of 56.67J/mm³.

The building orientation of the initial sample was horizontal meaning a 0° inclination respect to the base plate of the machine detailed see in Figure 10.

There are two important parameters for positive and negative microneedles that influence the geometrical accuracy for side variable. Fill contour (FC) and the border value used for this experimentation are presented in Table 6 continuously scheme displays shown in Figure 11. One border and two fill contours were configured for positive and negative constructions.

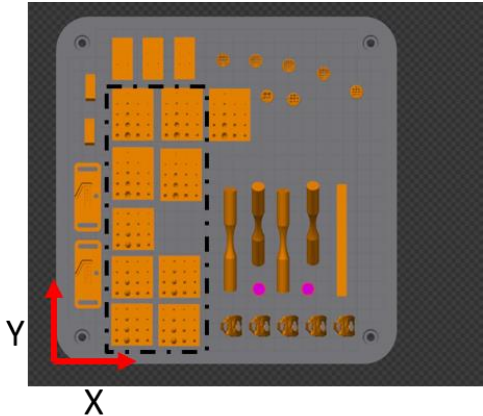


Figure 10. Configuration for initial samples in QuantAM software

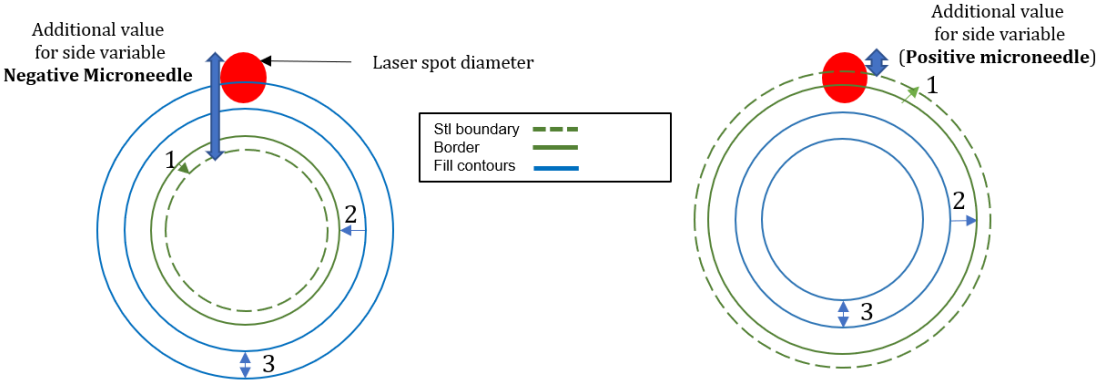


Figure 11. Representation of borders and fill contours in negative (left) and positive (right) microneedles construction

Table 5. Phase 1 parameters

Parameter	Value
Mesh	
Layer thickness	50 µm
Point distance	20 µm
Hatch distance	0,06 mm
Power	170 W
Exposure time	20 µs
Scan strategy	Meander
Contour and border power	170 W
Beam compensation	22,5 µm
Downskin	
Contour and border power	170 W
Material	Stainless steel powder SS 316L-0407

Table 6. Border and fill contour parameters

Enumeration	Parameters	Acronyms	Distance value
1	Beam compensation	BC	22,5 µm
2	Fill contour offset	FCO	60 µm
3	Fill contour distance	FCD	60 µm

In phase 2, a variation was done regarding the contour and border power with difference in value of 110 W and the other parameters were remained the same, more detail is in Table 7. The building orientation selected for the manufactured insert was horizontal at 0°; vertical at 90° and finally tilted at 45°. Modifications of the orientation and supports were carried out in QuantAM of Renishaw. Detailed explanations can be found in Appendix B: QuantAM preparation. Building orientations are shown in Figure 12.

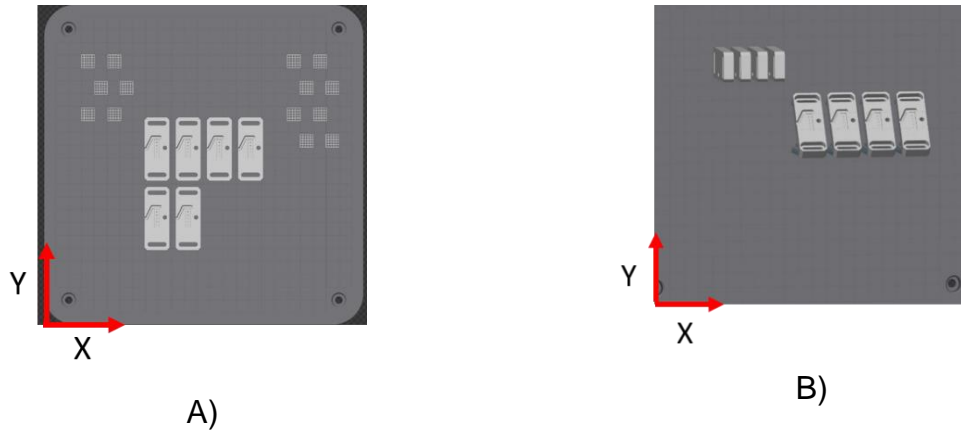


Figure 12. Inserts building orientation. A) 0° B) 90 °and 45° in QuantAM.
Software

After being manufactured, pieces with the SLM process were immersed in isopropyl alcohol with an ultrasound bath for 10 minutes.

Table 7. Phase 2 parameters

Parameter	A	B
Mesh		
Layer thickness	50 μm	50 μm
Point distance	20 μm	20 μm
Hatch distance	0,06 mm	0,06 mm
Power	170 W	110 W
Exposure time	20 μs	20 μs
Scan strategy	Meander	Meander
Contour and border power	170 W	170 W
Beam compensation	22,5 μm	22,5 μm
Downskin		
Contour and border power	170 W	110 W
Material	Stainless steel powder SS 316L-0407	

3.3.1.2 Parameters modification

For phase 2 the modification was based according the 3 build surface orientations studied 0° , 45° and 90° to improve the height accuracy.

For microneedles cavities at 0° , the building configuration has more energy density due to the laser steps in contours and borders (green and blue dots) than for hatching lines (yellow dots) as shows Figure 13 B. Also, Figure 13 A shows the configuration for microneedles. In this orientation they are conformed by upskin layers, which means the presence of areas where no solid material is present in a layer above [42]. Because the construction and to improve the quality in lateral cavity; 110 W of power was set in the contour and borders for the mesh.

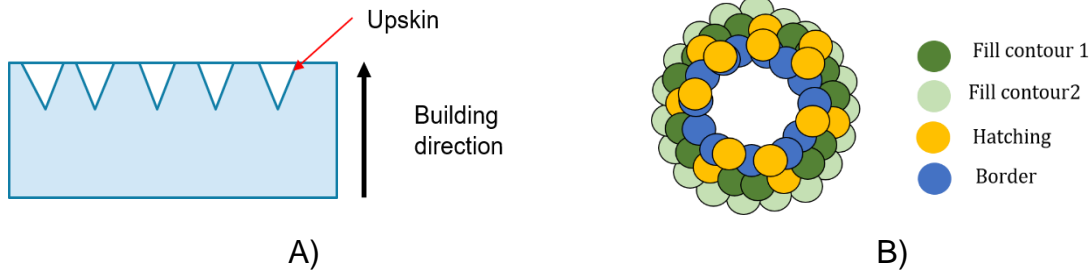


Figure 13. Layer configuration for microneedles at 0° of build surface orientation (A) and border and contours representation in conical base (b)

Microneedles cavities at 45° had an upskin configuration too, so the parameters were the same as 0° build surface orientation. However, for 90° orientations (Figure 14) microneedles had upskin which was defined before and downskin layer configurations which means zones where there is not material in the layers below [42]. It was found in literature a power of 110 W can improve downskin areas [43].

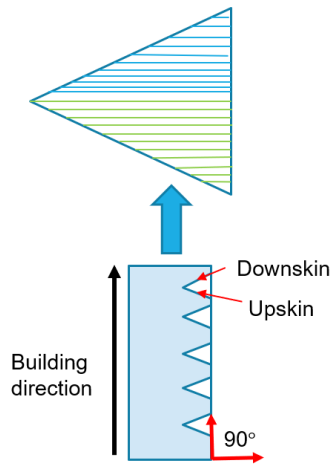


Figure 14. Layers configuration for microneedles at 90°

3.3.2 Digital light processing

Envision Tec Perfactory III mini multi lens was used to produce initial samples for negative microneedle characterization and for microneedle inserts. This equipment has a voxel size of 60 μm , a layer thickness of 25 μm was selected.

Initial samples were built at 0° respect to the building platform. However, inserts were manufactured at 0° and 45° as shows Figure 15.

After the pieces were manufactured in this process, the samples rest in a post curing process with oto flash equipment of Envision Tec with 2000 cycles and 10 pulses per second, more parameters for this technology can be found in Table 8



Figure 15. Inserts build surface orientations. A) 0° B) 45° in digital light processing

Table 8. DLP parameters

Parameter	Value
Layer thickness	25 μm
Irradiance	700 mW/dm^2
Voxel depth	50 μm
Voxel size (X and Y resolution)	60 μm
Post curing	2000 cycles
Post curing	10 pulses per second
Material	HTM 140

3.3.3 Characterization

Morphological characterization was carried out in Stereo Microscope Carl Zeiss v8, it provided a specimen three-dimensional view with typical magnification range between 20x and 50x. This type of microscope is ideal for amplifying opaque and thick samples from the fact that it uses reflected light from the object. The selected magnification in phase 1 was 1.0 X and 3.25 X in phase 2.

Dimensional characterization and surface roughness were carried out in Alicona infinite focus. Height and base length for positive and negative constructions represented in Figure 16 were measured with parameters displayed in Table 9.

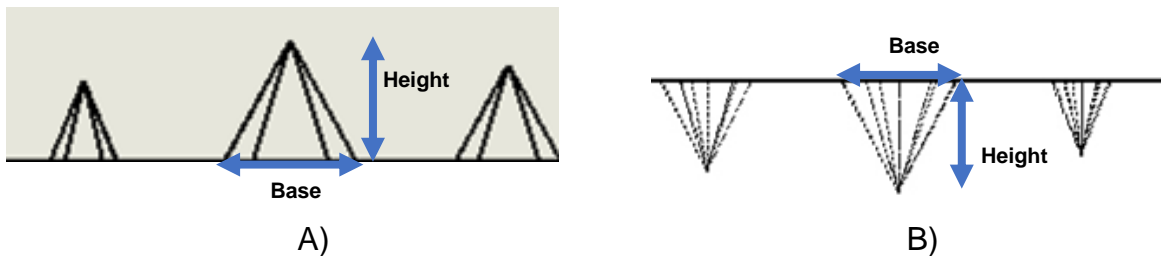


Figure 16. Representation of variable for a) positive and b) negative constructions

Four height measurements were made from each microneedle as indicated in Figure 17 and Figure 18 for length sides; for figures with side number greater than 4, sides were chosen randomly.

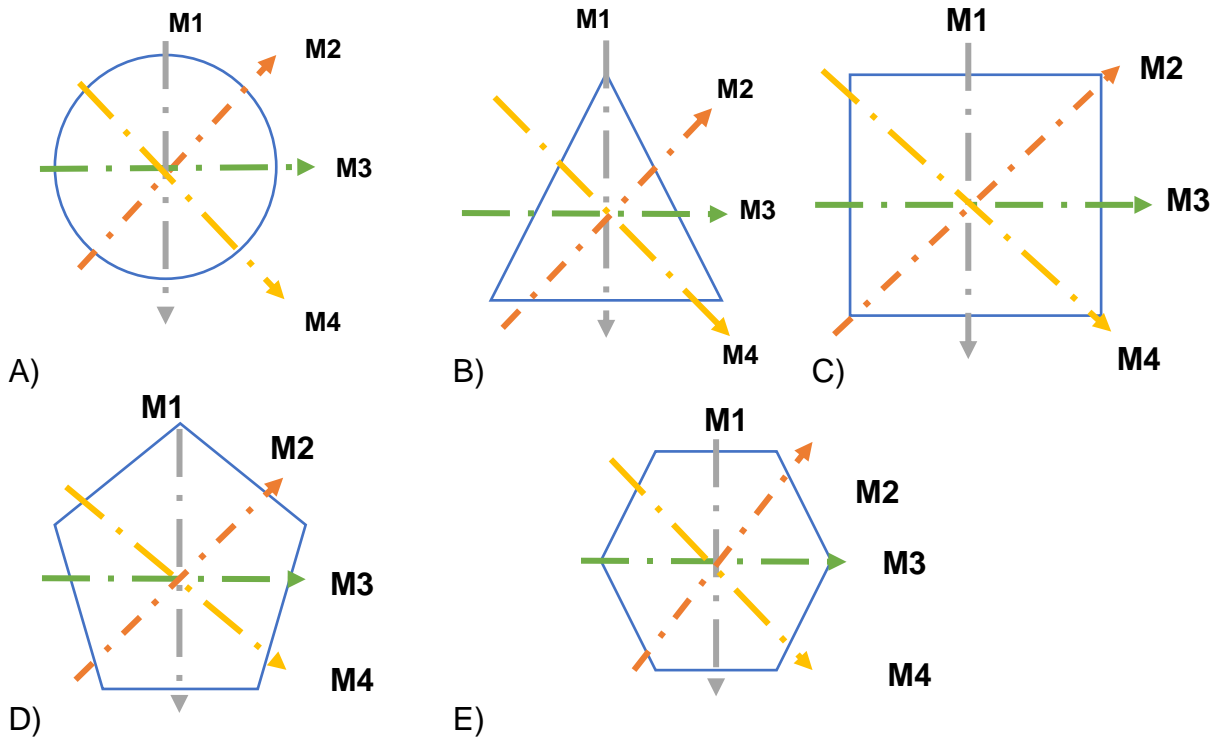


Figure 17. Height measurements representation for bases a) conical, b) triangular, c) square, d) pentagonal and e) hexagonal

For tip radius, one measurement was taken for positive construction of microneedles. The contour measurement module was selected to take a cross sectional view of the highest part of the microneedle and then it was measured as indicates in Figure 19.

Table 9. Alicona parameters

Process/ parameter	Phase 1 SLM	Phase 1 DLP	Phase 2 SLM	Phase 2 DLP	Surface roughness SLM
Magnification	5X	5X	10 X	10X	5 X
Objective					
Exposure	6,7 ms	140ms	3 ms	124ms	3 ms
Contrast	1	1.27	1	1.27	1
Vertical resolution	0,84	0,84	0,84	0,84	3
Lateral resolution	2,8	2,8	2,8	2,8	12

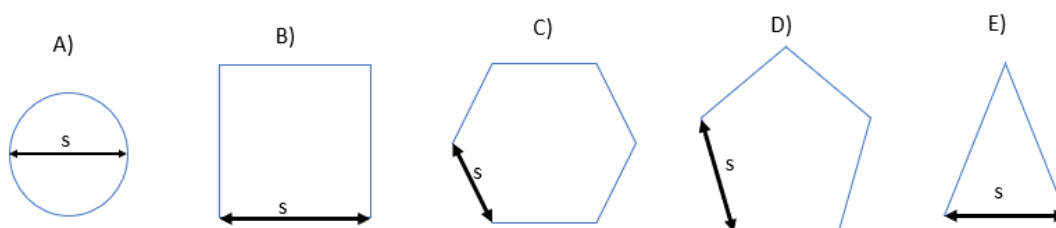


Figure 18. Side lengths measurements representation for bases a) conical, b) square, c) hexagonal, d) pentagonal and d) triangular

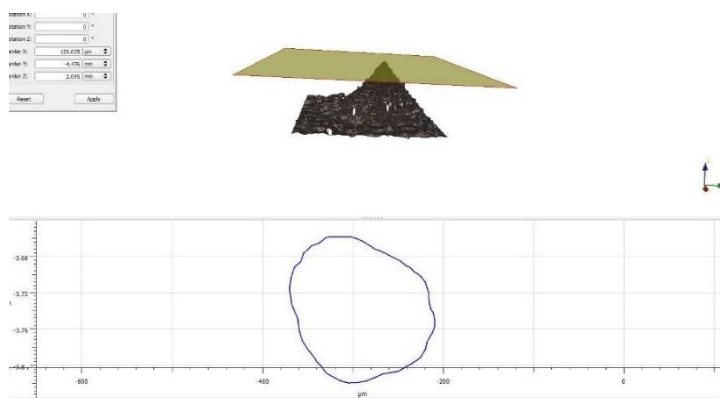


Figure 19. Tip radius measurement

Microneedle insert measurements were carried out in two positions for the runner. One was on the top position respect to the Alicona lens as shown in Figure 20 and the second one was in lateral position respect to the Alicona lens seen in Figure 21. Measurements of thickness, height and width were carried out with a Mitutoyo Vernier Caliper.

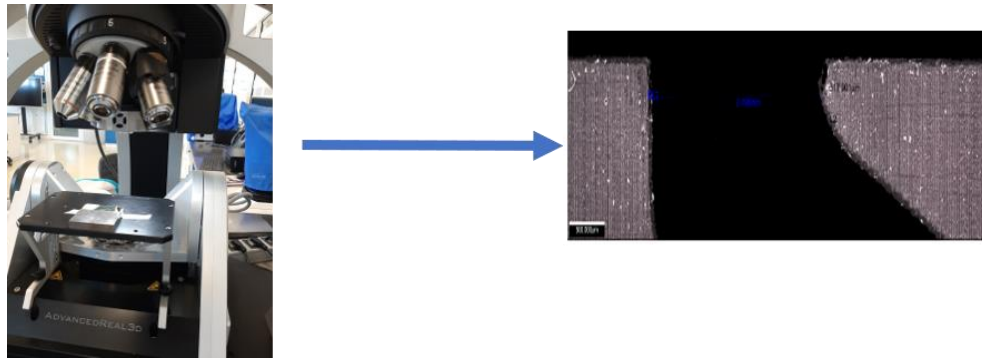


Figure 20. Top side measurement for runner

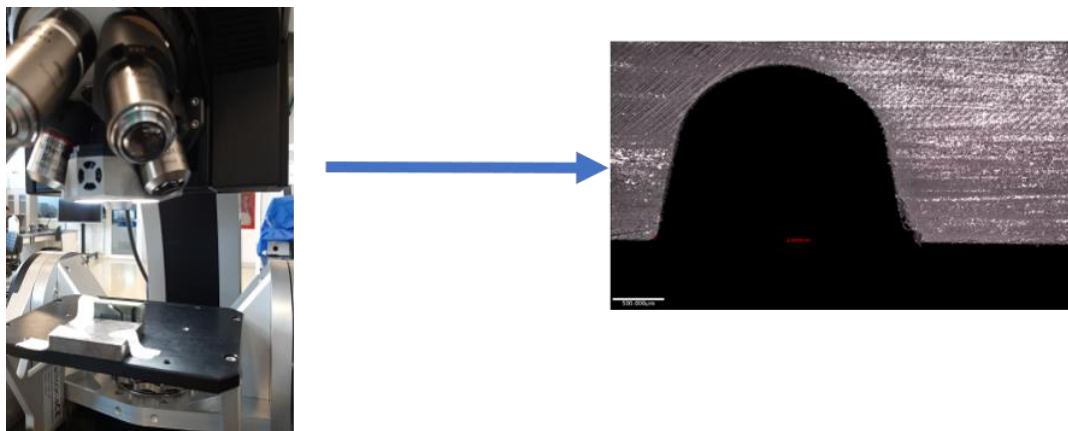


Figure 21. Lateral side measurements for runner

Chapter 4

4. Results and discussion

4.1 Phase 1 Results

4.1.1 SLM: Microneedles bases characterization for positive and negative constructions.

Figure 22 below shows the average height measurements for the negative and positive constructions. These results suggested initially that positive microneedles had a better dimensional accuracy in height variable in contrast to negative microneedles which had lower precision respect to the nominal value. It should be notable that none of the bases for the negative group reaches CAD input value with this technology.

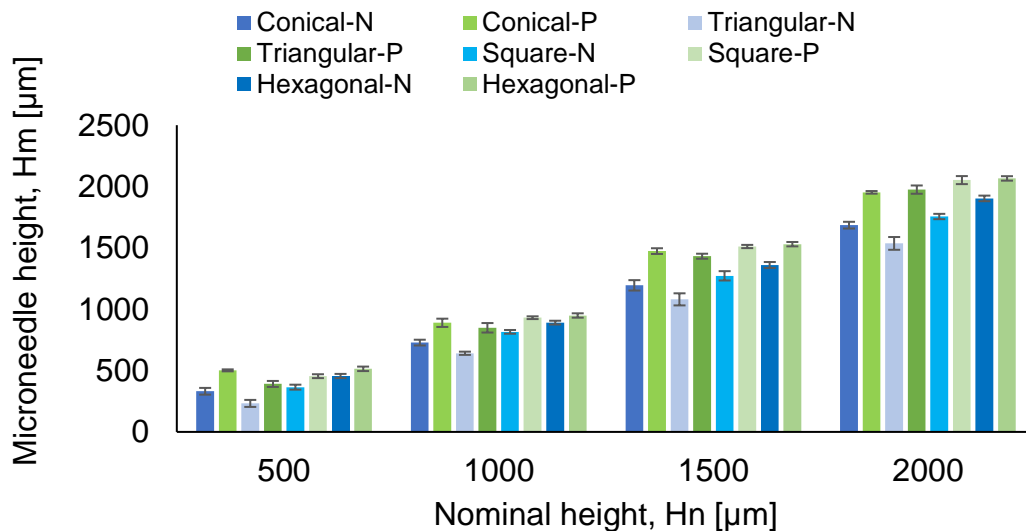


Figure 22. Microneedle height for positive and negative constructions in SLM

Others like Ahmed et al. [44] studied height variable for positive rectangular samples manufactured by the SLM process but applied in another material as AlSi10Mg. Their findings determine fewer values than the nominal CAD input with a

maximum error of 1.562%. They also performed an ANOVA study concluding that; respect to the height, implicates statistical differences under repeated conditions.

This variation in microneedle height for both constructions; positive and negative, can be explained due to the location of the z axis in the sample construction. Along this axis the platform moved during the fabrication and led to an error. In addition, microneedle tips could not be achieved because the laser spot size had a minimum feature of 70 μm . That is the reason not all the layers were built for this design thus height was not reached at all. Although, there were higher values than the nominal for positive microneedles due to the laser penetrated more deeply into the unwanted bond powder particles. In contrast, thermal stresses impact on height variable, led to had lower value for the negative construction.

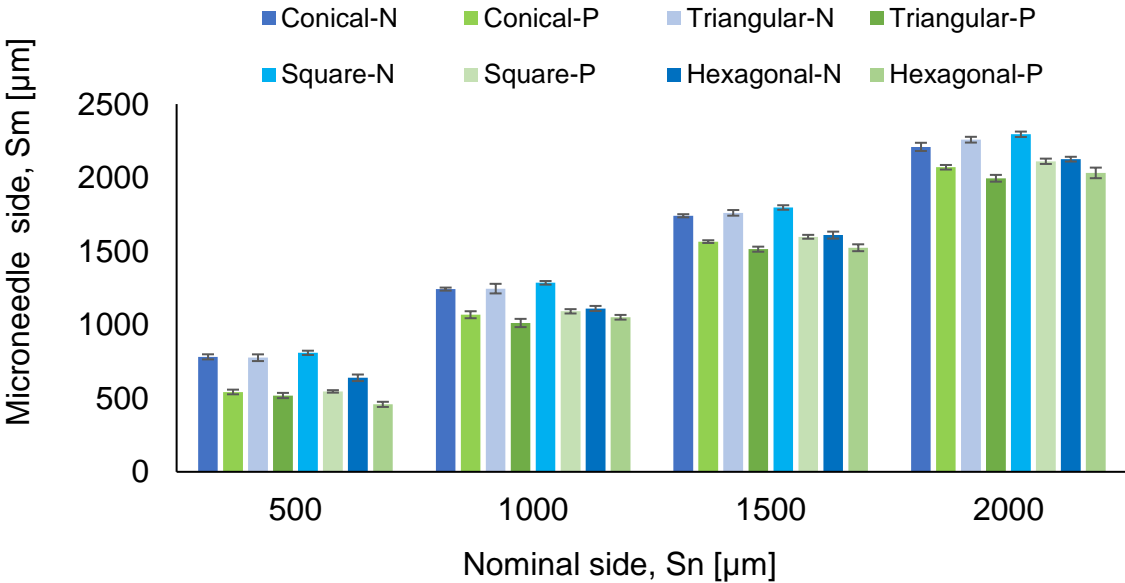


Figure 23. Side results for positive and negative constructions in SLM

Figure 23 displays better results for measurements of side variable than height. For positive microneedles building, accuracy in X and Y planes was better than negative microneedles. It is interesting to note that the higher values for negative microneedles can be related to the geometry in the building configuration explained in section 3.3.1. For positive microneedles, the border and fill contours were built from outside to inside respect to the STL boundary. On the other hand, for

negative microneedles, this configuration was built from inside to outside respect to the STL. This means that the values of beam compensation; fill contour offset and fill contour distance, affect the side measurement. There is possible to sum these values to calculate the additional dimension Figure 24 B. Furthermore, it is necessary to mention that for corners in triangular, square, pentagonal and hexagonal bases add an error to the side variable because the laser beam builds a bigger geometry as is shown in Figure 24 A obtained from QuantAM software.

$$\text{Equation 1. } \left[\text{Beam compensation offset} + \text{fil contour offset} + \text{fillcontour distance} + \left(\frac{\text{spot size diameter}}{2} \right) \right]$$

As an example, the square base for negative microneedle design had an additional side measurement of 180 μm which was choose with a red arrow in Figure 24 B and corresponds to Equation 1. That value corresponds to an ideal square geometry. However, the laser is not able to obtain the perfect corner of the square. The laser adds a curvature which represents 75 μm more for the side variable. In the end, it will be expected to obtain a measurement of 330 μm additional to the nominal value.

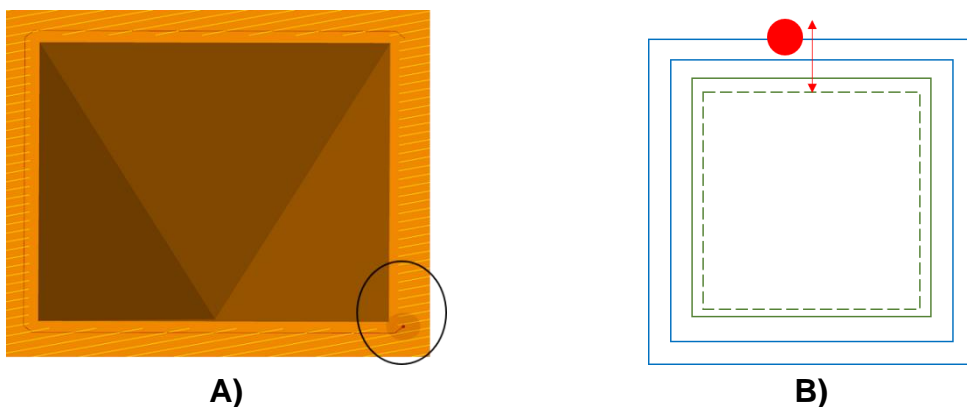


Figure 24. Corners configuration for negative microneedles square sides
a) QuantAM software and b) Ideal square geometry

About the increment in side variable measurement, other researchers have reported for example, Sabina et al. [45] carried out an investigation with selective laser melting in Maraging steel, reinforced with cobalt. This research talks about dimensional capabilities in holes and extrusions of parallelepiped. The maximum dimensional error was 20% for diameter variable. Kniepkamp et al. [46] studied the dimensional accuracy of micro parts manufactured with selective laser melting in Stainless steel. This author found that, for radius of 30 μm and chamfers; differences allocated up to 30 μm and demonstrated that by increasing the laser power, the mean deviation increased. Zhang et al. [47] studied the horizontal dimensional accuracy with a prediction model showing that this variable was composed by two stages. First one refers to the track filling and the second one to the track width. This investigation used a compensation value to obtain an accurate result.

Figure 25 displays more information about the relative error of height microneedles for each of the configuration designs positive and negative. It shows that for negative construction, there was a bigger relative error percentage with a maximum value of 36.18%. Elseways in positive design, it had a better dimensional precision with a maximum error of 14.45% of relative error for this variable. The relative error was obtained from

$$E_r = \left| \frac{\text{Nominal value} - \text{Measured value}}{\text{Nominal value}} \right| * 100$$

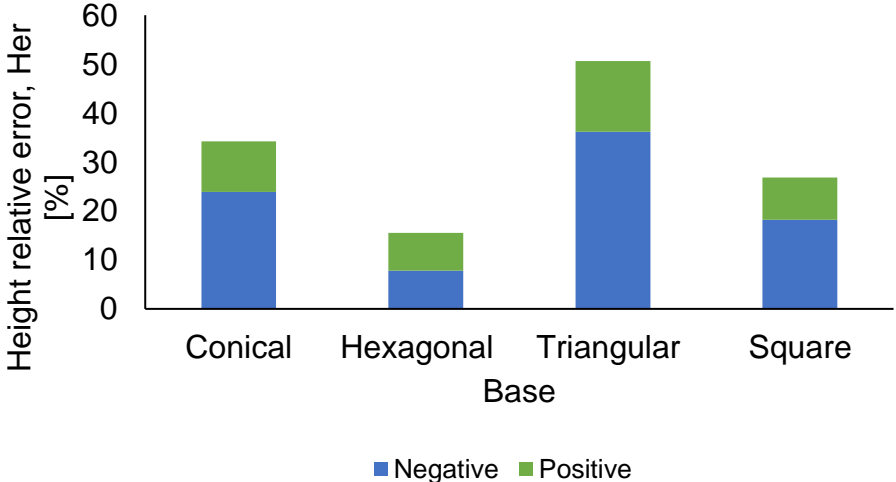


Figure 25. Relative error for height variable

Figure 26 confirm that side variable for a positive microneedle manufactured with SLM had better dimensional accuracy than negative retrieved from data which exhibited a maximum relative error of 33.06% and 6.76% for positive and negative microneedles, respectively.

Respect to base designs considering side and height variable, the hexagonal base had lower relative error. Therefore, this had the best dimensional accuracy. Contrarily, the worst design was microneedles with triangular base.

For height variable in microneedles with negative construction, it was necessary to consider the moment the laser builded the first layer because excessive material could had been molten and the cavity was not formed afterwards considering the area was too small when the tip inversed was manufactured.

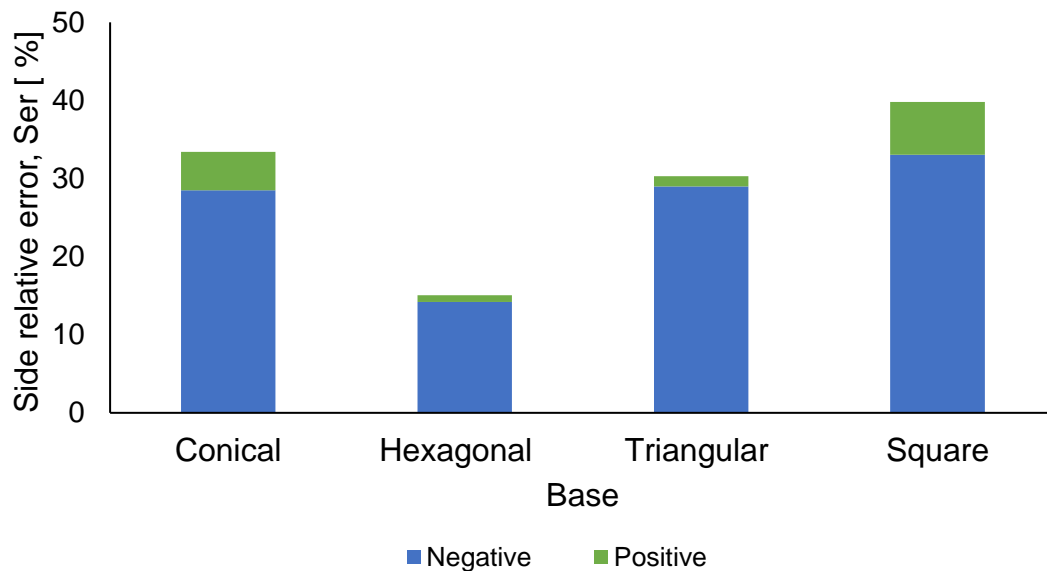


Figure 26. Relative error for side variable

This result confirms previous studies for this research, the length variable had lower dimensional accuracy (Z axis laser construction) than the side variable (X and Y axis laser construction) [44]. Also, according to literature, this can be achieved as result of thermal residual stress effects are longer in the Z axis perpendicular to the scanning direction than for X and Y scanning direction plane [48].

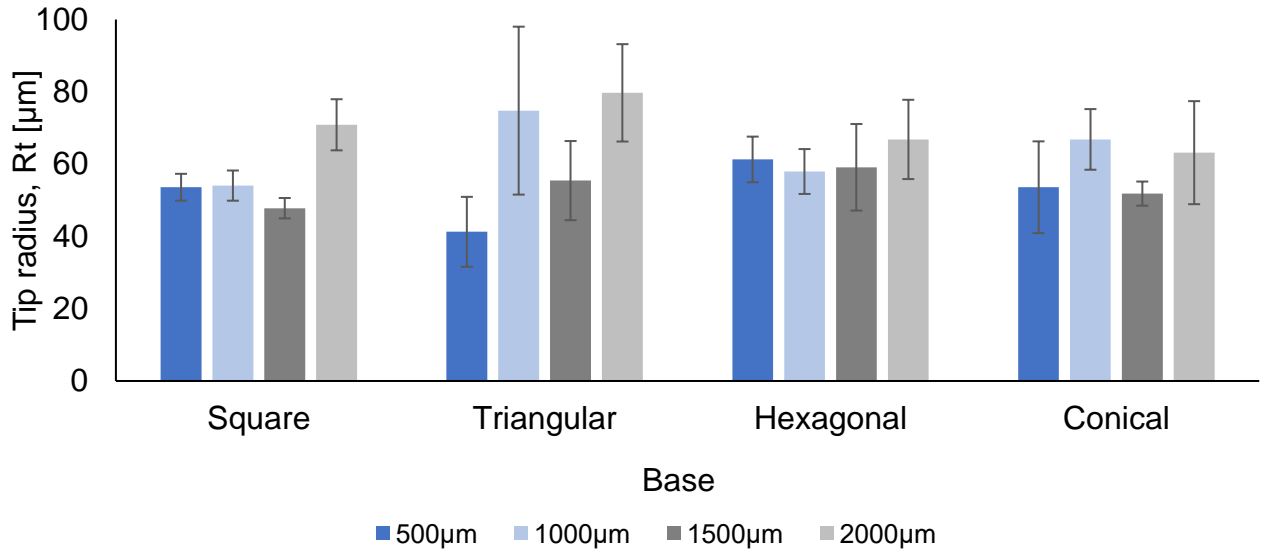


Figure 27. Tip radius for positive microneedles in selective laser melting

Figure 27 shows the results for tip radius obtained for different. Literature has reported tip radius values for other processes for example Nair [18] produced inserts with EDM technique. Those were tested in PDMS polymer casting with tip radius of $32 \pm 8 \mu\text{m}$. Krieger et al. [5] used the SLA process with a tip radius between 20 and 40 μm . Gittard et al. [34] reported micro stereolithography dimensions with tip dimensions of $90 \times 30 \mu\text{m}$. Johnson and Procopio [33] used DLP microneedles with tip radius range from 40 μm to 160 μm . Gulcur et al. [49] used the micro injection molding technique with tip radius results of 40 μm ; a maximum needle tip diameter of 188 μm was reported in dry cutting micromachining process by López et al. [17].

Compared to other microneedles manufacturing investigations, the tip radius for SLM is located in the value range reported which is possible because of the minimum size feature obtained was 70 μm . The average measured of the pool molten width was 102 μm which according to the setting parameters, the addition of spot diameter and beam compensation was 97.5 μm . Half of this value is similar to results obtained for tip radius in Figure 27.

Contrary to the findings of Krieger [5] where microneedles were manufactured with stereolithography; the tip radius decreasing tendency did not decrease at a

lower height value. In this research, for selective laser melting technology tip radius were similar and stable among different heights.

The accurate range reported in literature for a successful insertion into the skin is from 2.3 -50 μm . Actually, with selective laser melting it is possible to get the maximum value of 50 μm [8] [50] [51] [14].

4.1.2 Optical characterization of microneedles in positive construction

Figure 28 shows lateral images for positive microneedles with heights from 1000 – 2500 μm . It was observed powder adhesion in the lateral surface. The lower heights were obtained with conical and triangular bases in figure A-D and E-H, respectively. An increase in the side number resulted in a higher accuracy for height variable measurement.

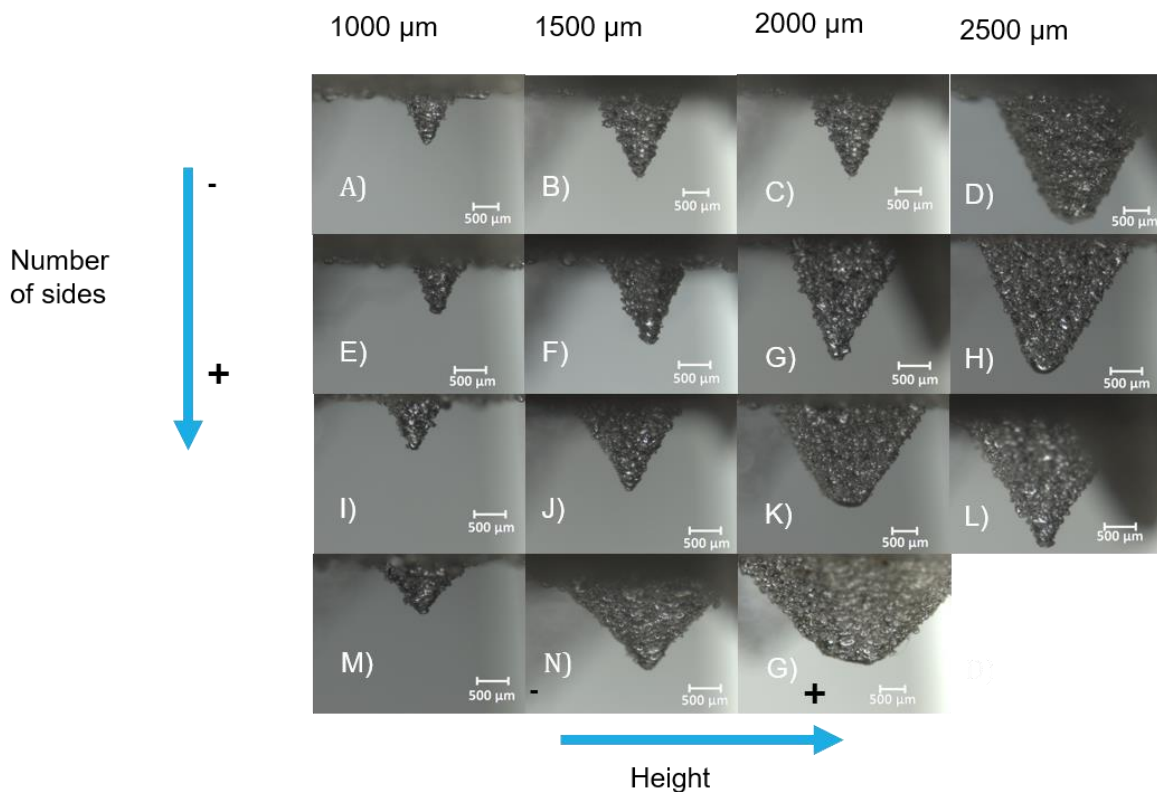


Figure 28. Lateral view in microscope for heights: from 1000 μm to 2500 μm for bases conical (A-D), triangular (E-H), square (J-M), hexagonal (N-P)

4.1.3 Digital light processing: Microneedles bases characterization for negative construction

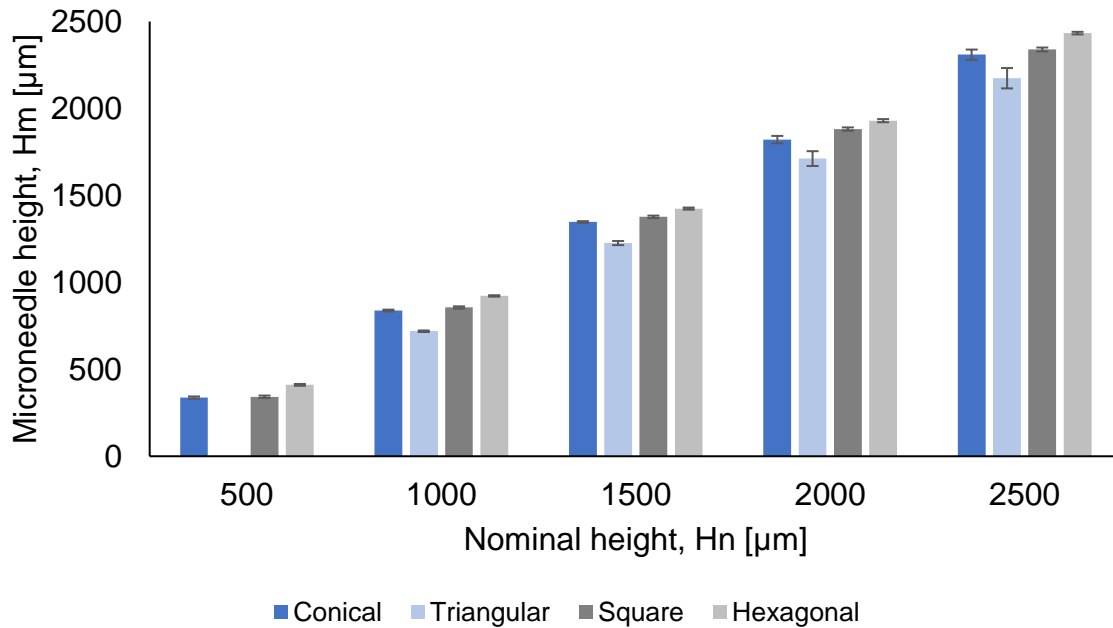


Figure 29. Height results for negative construction in digital light processing

Figure 29 represents the results of average roughness and standard deviation for height variable studied for negative microneedle design. Positive design was not studied because there has been a lot of research towards this technology. Results for this technology are good for example the hexagonal base the best configuration design in order of maximize dimensional accuracy because it had the lowest difference respect to the nominal value with the following results: 410.56 μm, 921.95 μm, 1424.25 μm, 1929 μm and 2433 μm for nominal values of 500-1000-1500-2000 and 2500 μm respectively. The lowest values were obtained with the triangular base design and the highest results correspond to the hexagonal base. Its performance is similar to the SLM technology in terms of height. That can be explained cause the hexagonal base cross-sectional area is higher. So, the technology can project more layers for a hexagonal configuration in the photopolymer resin.

Heights results for negative microneedle design however had disparity to the nominal value. Similar differences were obtained by Johnson and Procopio [33] and Gittard et al. [34] for microneedles height. Both suggested that it could happen by effects such as diffraction and refraction. These results confirm the Johnson and Procopio theory: it is normal for light reflected to spreads into the nearest pixels consequently increases the amount of light per unit area in large parts. On the other hand, for small parts as microneedles tips, these areas are not cured so the microneedle height can be affected when the structure width decreases enough to reach a minimum light intensity for curing. This can be happened in the triangular base specifically where the minimum feature design of 500 μm was not obtained considering that this geometry has the lowest cross-sectional area.

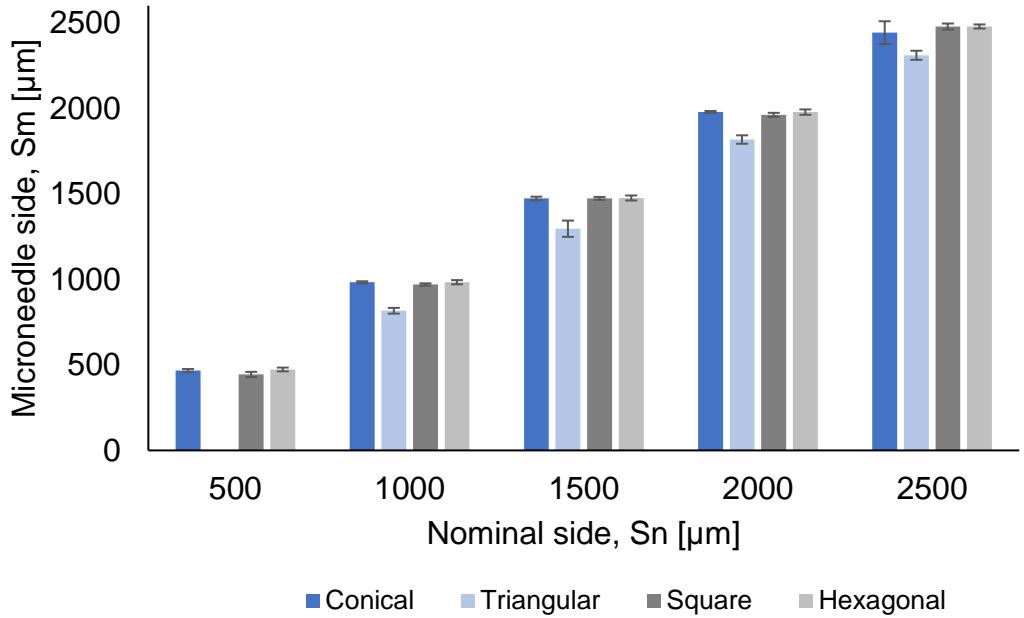


Figure 30. Sides results for negative construction in digital light processing

As Johnson and Procopio experiences [33] side variable had closer fidelity with nominal values including the minimum value of 500 μm as shows Figure 30. Hexagonal base design had the best dimensional accuracy with average values of 473 μm , 983 μm , 1475 μm , 1977 μm and 2478 μm for nominal values of 500-1000-1500-2000 and 2500 μm , respectively.

The lowest dimensional accuracy for this variable was obtained with the triangular base configuration.

4.1.4 Selective laser melting and digital light processing height relative errors

Figure 31 and Figure 32 shows results for the average absolute error of each geometry and nominal height for SLM and DLP technology, respectively. It is noticeable that for both technologies, hexagonal geometry was the best design with the lowest relative error considering the same nominal height in all categories. A tendency was found that triangular bases obtain higher relative error.

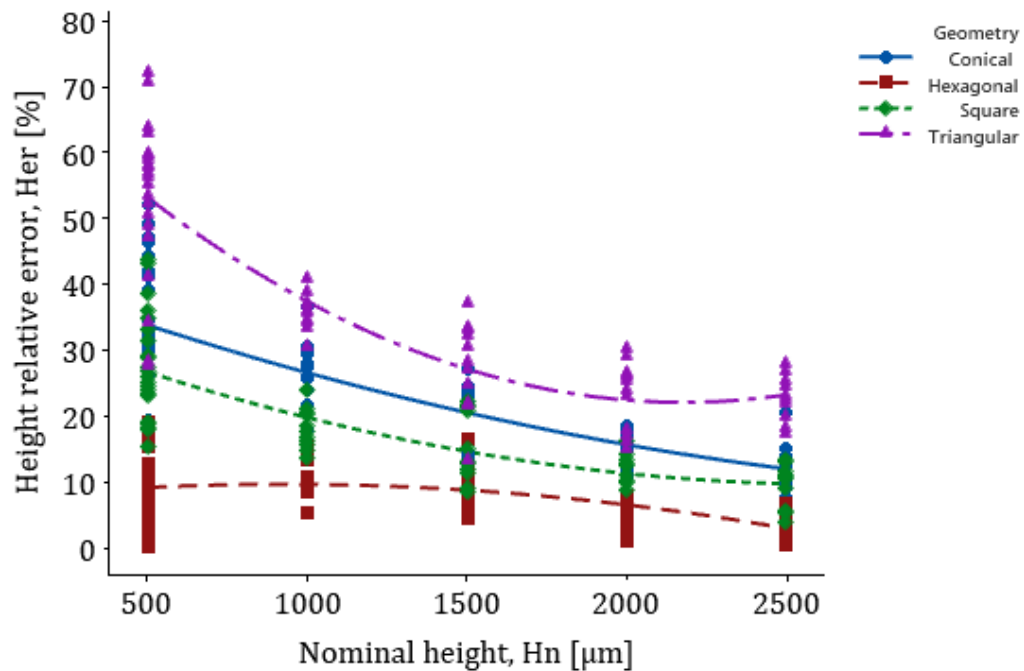


Figure 31. Capabilities for height variable in negative construction for SLM technology

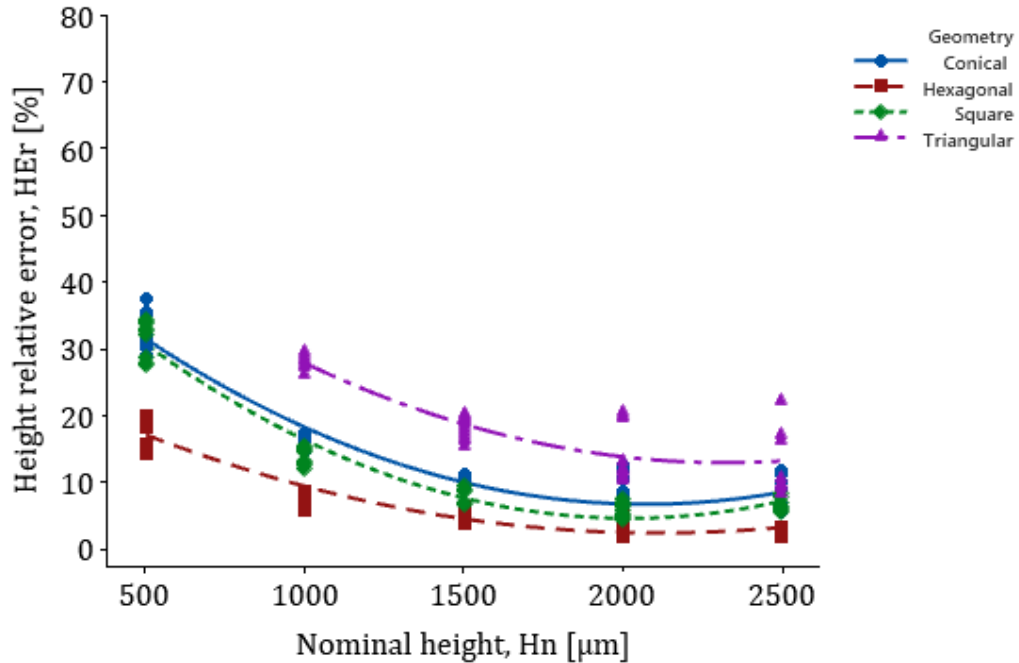


Figure 32. Capabilities for height variable in negative construction for DLP technology

From graphs it is able to dictate that geometry has a significant effect on height accuracy. This can be explained due to a factor call “stair stepping” (Figure 33). This have been reported in literature for both technologies: digital light processing and selective laser melting [33] [52] [9] [5] [53]. Others additive manufacturing technologies such as material jetting processes have reported this same phenomenon [54]. This factor produced elevated edges in lateral surfaces of microneedles. When it is more noticeable leads to the obstruction of the final cavity therefore to a reduction in height value.

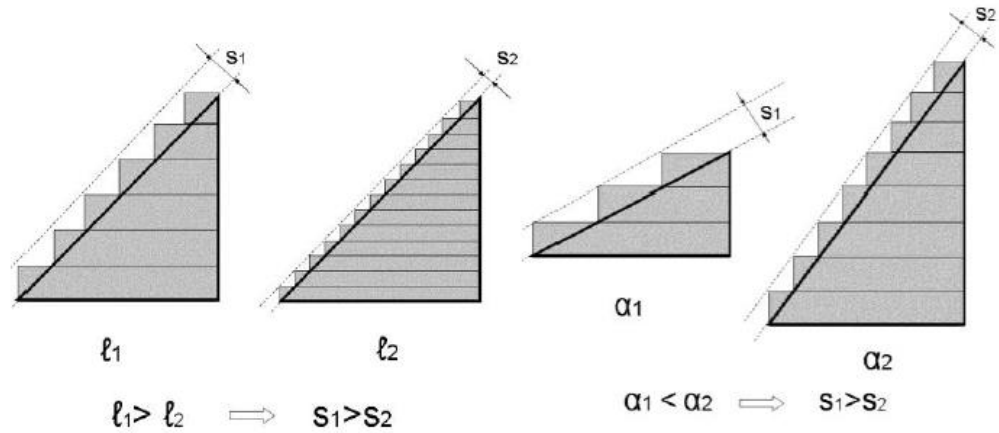


Figure 33. Stair stepping effect for layer thickness l and building angle α .
Retrieved from [55]

Stair stepping is common for both process because the fabrication method is by layers. An author reported an improvement with a reduction in the layer thickness for DLP process [5]. Others as Jhonson and Procopio [33] applied an antialiasing algorithm which improved the height accuracy. Also, this factor is presented for both technologies because it takes place when a surface orientation is not orthogonal to the axis of the source energy being the case for microneedles cavities fabrication [54].

Two variables can improve this stair stepping effect: first with the reduction of the layer thickness and second the increment of the geometry angle. By increasing the number of sides for the geometries bases, increased the value of the angle. That explain why conical and triangular bases had the worst errors shown in Table 10.

This angle is calculated respect to the horizontal which is the previous layer (Figure 34). When the build surface orientation changes, geometry angles kept the same order and therefore the tendency. Although the lowest angle value is for the conical base, the triangular base had the worst error indicating that the cross-sectional area is also relevant. Triangular MN have lower area than conical MN.

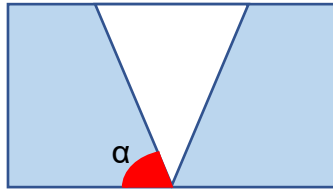


Figure 34. Angle for lateral microneedle cavity

Table 10. Angles for different geometries

Base geometry	α (°)
Triangular	64.34
Conical	63.43
Square	65.90
Pentagonal	67.614
Hexagonal	69.2

Appendix E: Relative error graphs, displays more information of over dimensional and sub dimensional errors for both technologies detailed for each variable studied in this research.

4.2 Phase 2 Results: Insert manufacturing with selective laser melting and digital light processing

Initially, to study build surface orientation, the experiment was carried out with the parameters examined by Cedillo et al. [41]. Figure 35 shows results for average height variable in the microneedle insert manufactured with selective laser melting and digital light processing. The highest average value was obtained with the hexagonal base with 555.98 μm representing a difference of 44.02 μm in comparison with the lowest of 240 μm with a difference of 360 μm respect to the nominal value for the triangular base. These results confirm the afore mentioned in section 4.1.1 which mentioned the best dimensional accuracy obtained corresponded to the hexagonal base and the worst to the triangular base.

Figure 35 shows a possible relation for SLM and DLP between the increment from 0° to 45° and the output height improvement. A non-parametric test was carried out to find differences among the buildings orientations groups. Only for DLP process

with 45° orientation proved that it had a greater height than 0° orientation. The null hypothesis that medians of both groups were equal to zero was rejected with a P value of 0.048 with $\alpha = 0.05$. This can be explained due to the cross-sectional area for 45° microneedles is greater than 0°. This variable improved the height accuracy due to the projection area is greater and solidification did not occur as fast as small areas.

In contrast, the SLM process did not find any differences between orientations of 45° and 0°. The null hypothesis was not rejected, with a p value of 0.329 and a significance level of 95%. For building orientation of 90°, SLM results suggest lower values in comparison to the other orientations. Orientation for SLM technology did not influence on height accuracy.

Figure 36 shows that only for 0° orientation, the design was similar to the CAD; in comparison to the 45° and 90°. There was not possible to identify the accurate geometry because the inclination angle affected the figure structure.

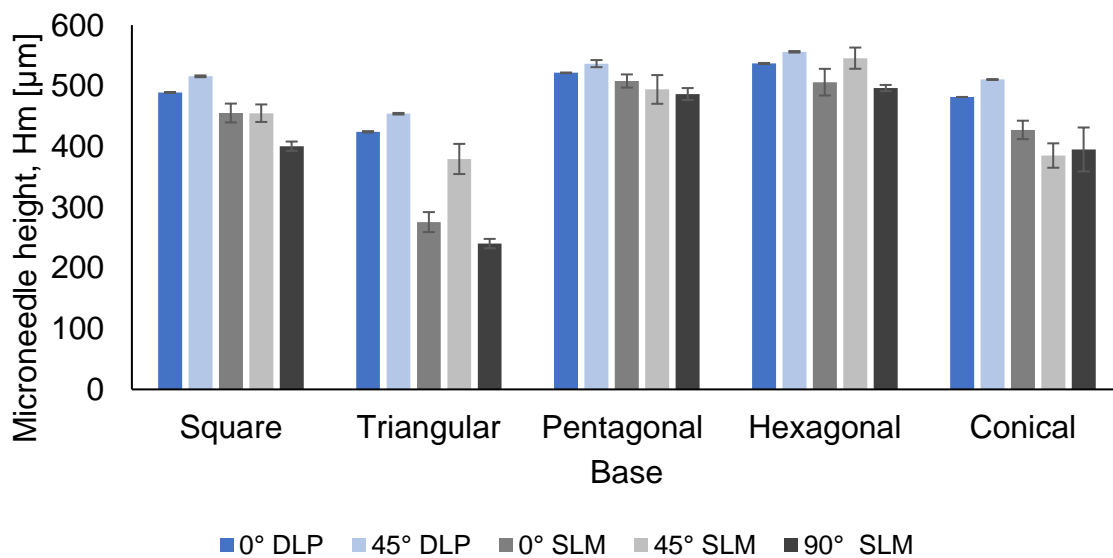


Figure 35. Height results for microneedle insert

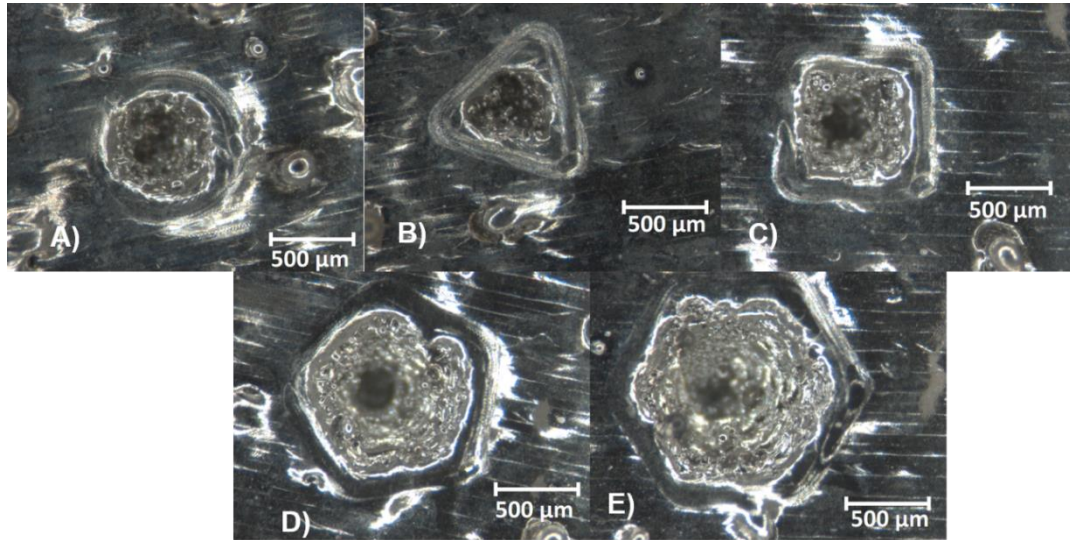


Figure 36. Top View for microneedles bases in 0° build surface orientation
A) conical, B) triangular, C) square, D) pentagonal, E) Hexagonal

Figure 37 show results for the side variable in the microneedle insert, results are a confirmation of sides for 45° and 90° orientations were shorter than the nominal value in the selective laser melting process. For 0° , sides are greater than the nominal value as was explained before in base characterization section. For the DLP technology this variable is more accurate. In Selective laser melting process this variable can be improve with parameters of borders, beam compensation and contours.

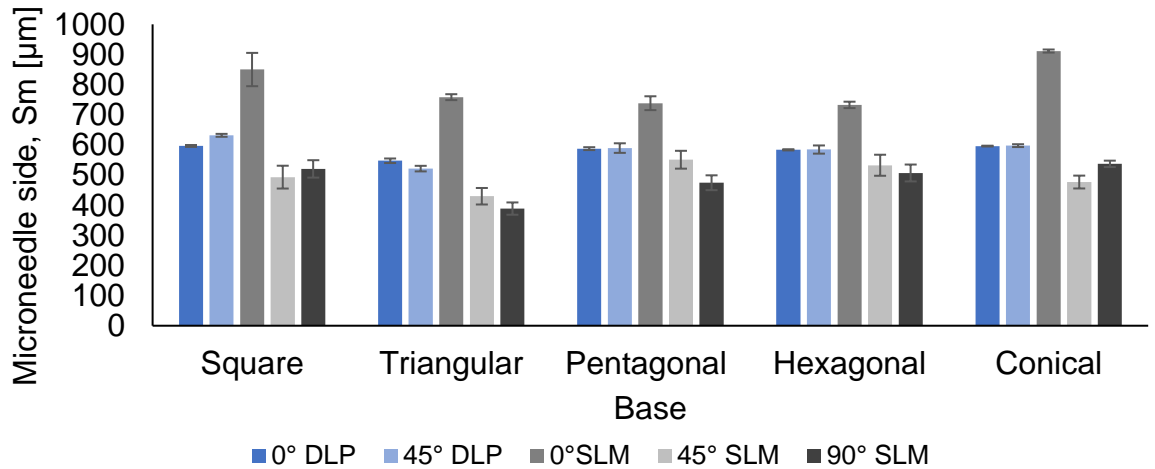


Figure 37. Side variable for Microneedle insert

Figure 38 shows the construction for hexagonal geometry sides at different build surface orientation. Graphs suggests that for 0°, the side formation did not change with the increment of the number of layers, compared to 45° and 90° (Figure 38 B and C). The side variable was built on a non-uniform way. This means when a new layer is formed, a part of the side is also fabricated until finishing the hexagonal base geometry. That configuration explained the reduction of side length increasing the slope angle.

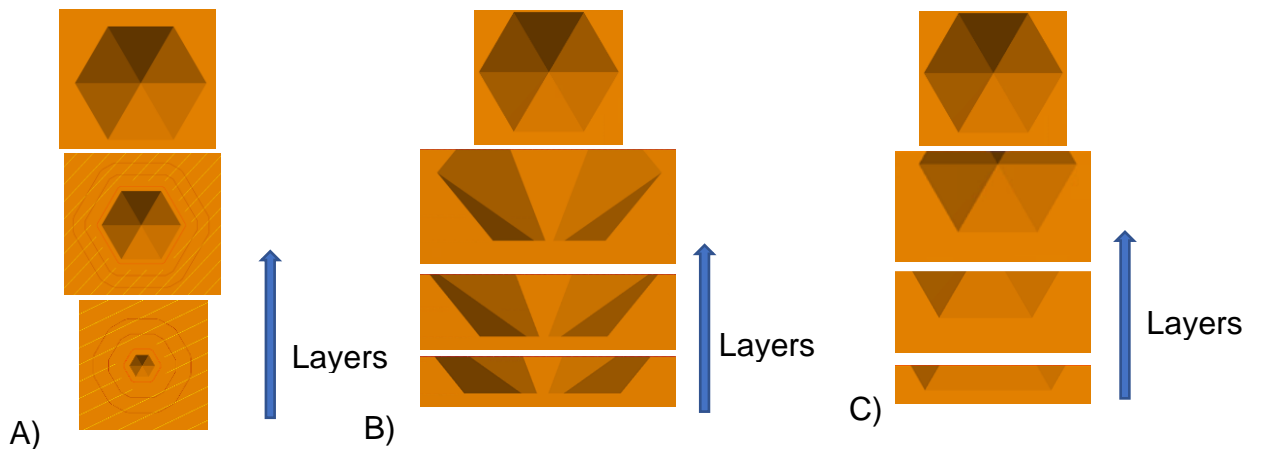


Figure 38. Hexagonal base geometry construction at A) 0°, b) 45° and C) 90°

Figure 39 show values for top average roughness measurement with 0° orientation with the highest value (23,93 μm) obtained compared to other orientations. There is a noticeable tendency when the inclination angle increased, the Ra value improved. It is similar to the reported in literature with overhanging parts Shi et al. [43] and Alrbaey et al. [56] Also this demonstrated that by increasing the fabrication angle, the Ra reduced.

An explanation of the reduction of the surface roughness is by effect of the energy density per layer studied by Rashid et al. [57]. His theory suggested a that the printing area is proportional to the energy per layer. This theory was confirmed in this work at the time the microneedle insert was fabricated at 0° since it had the biggest area therefore the biggest energy compared to 90° orientation with the lowest area per layer constructed.

A bigger energy density leads to defects as balling. Figure 40 and Figure 41 confirmed that idea. It is possible to observe bigger sizes at 0° for balling formation than for 90°. A reduction in height peak is noticeable from 150 μm in the 0° orientation up to 60 μm in 90° orientation.

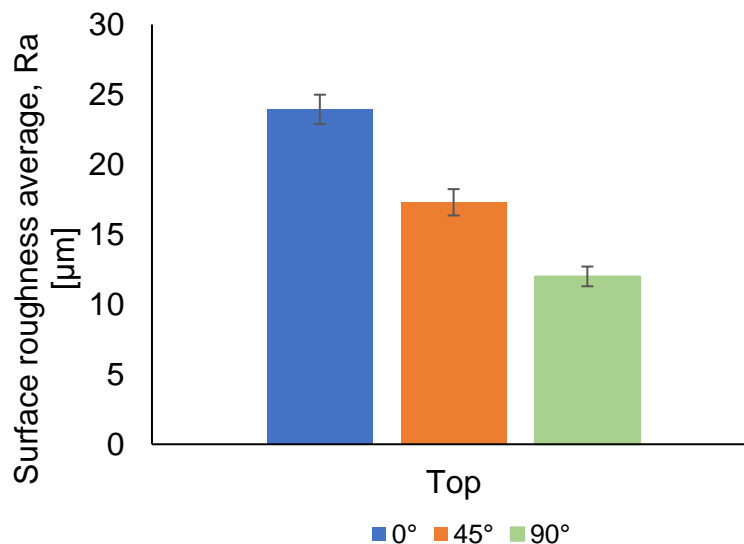


Figure 39. Top surface roughness average value

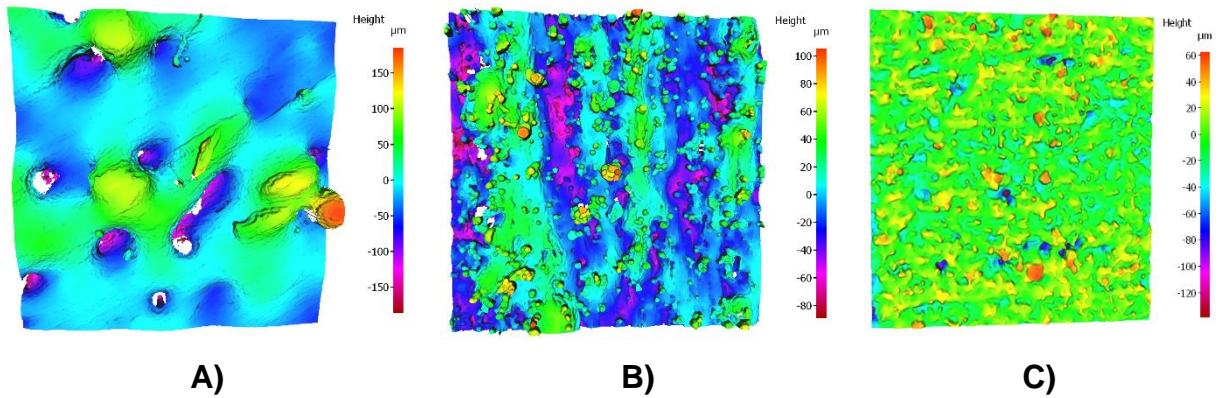


Figure 40. Surface topography for build surface orientations. A)0° B)45°
C)90°

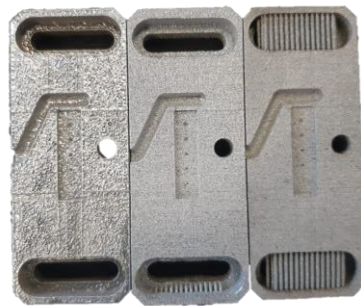


Figure 41. Microneedles inserts from left to right at 0°,45° and 90°

Although for this research, the 0° orientation surface roughness value did not achieve good results. Other researchers have studied parameters that improved top surfaces having a normal vector parallel to the fabrication axes [9] [58]. They found that for lower hatch space distance and lower point distance, drop higher overlapping percentages influencing significantly the Ra value since it allowed a stronger bond between layers and fusion of powder particles [59]. Also, SLM remelting has been investigated for enhancing surface quality. Pores which are formed between nearest melt pools disappear with this method [59] [60] [61].

For this research preliminary experiments were carried out to reduce surface roughness average with electropolishing in Appendix C: Preliminary electropolishing studies.

A new set of parameters was tested in microneedle insert to see if there could be an improvement in dimensional accuracy in height for small parts. For this section, contour and border power reduced down to 110V along with a density reduction from 226 J/mm³ to 146 J/mm³. From the fact that for this phase, different build surface orientation were studied; a reduction in energy density needed to be done in order to decrease the effects of underside overhanging surfaces to prevent burn through as other investigations quoted [43].

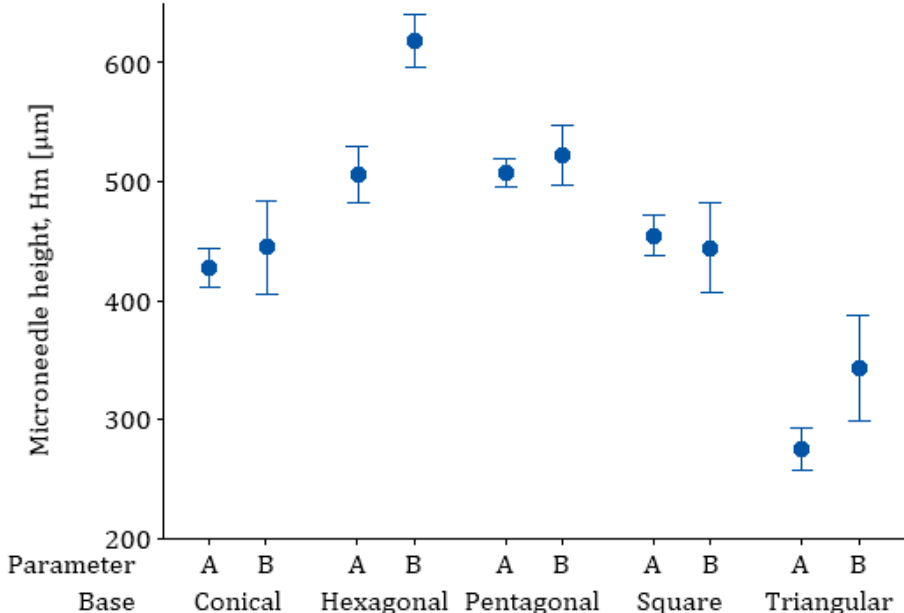


Figure 42. Parameters comparison for height variable in build surface orientation 0°

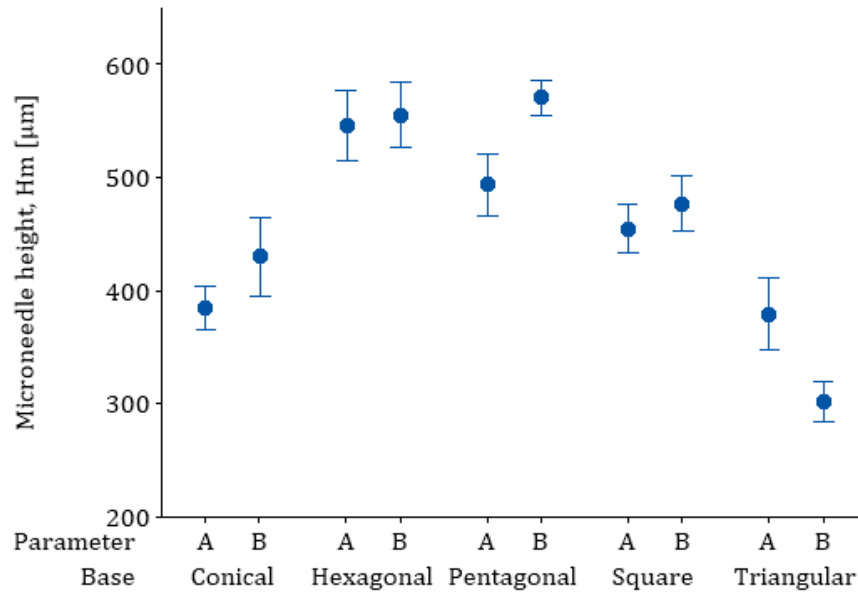


Figure 43. Parameters comparison for height variable in build surface orientation 45°

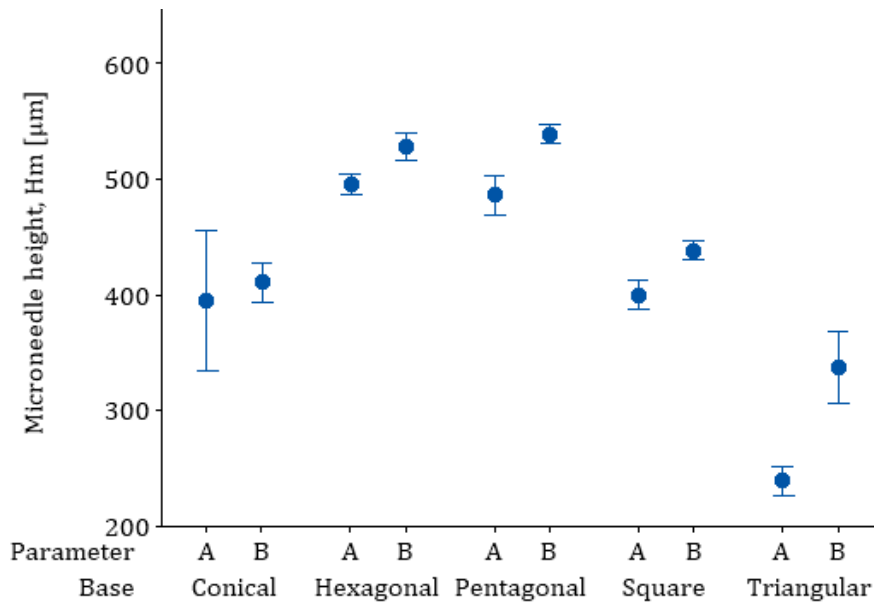


Figure 44. Parameters comparison for height variable in in build surface orientation 90°

Figure 42, Figure 43, and Figure 44 shows results for designation “A” based on Ramirez Cedillo et al. [41] and “B” being the parameter proposed. Both were

described in methodology section. Results suggested for both parameters that the hexagonal base was the best for height variable response. Furthermore, it seemed that parameter B was better than Parameter A. A hypothesis test was carried out in minitab with a confidence level of 95% in order to test the null hypothesis that means of height for parameter A are equal to parameter B. On the other side, the alternative hypothesis is that the mean of height for Parameter A is less than for parameter B.

For the group of 0° just the hexagonal and triangular bases rejected the null hypothesis with P values of 0 and 0.006 respectively as Figure 42 shows. For the group of 45° orientation just for the pentagonal and conical bases rejected the null hypothesis with P value of 0 and 0.010 respectively as Figure 43 shows. However, for the 90° orientation for every base except the conical one, demonstrated the alternative hypothesis as Figure 44 suggests. In addition, the P values of triangular, square, pentagonal, and hexagonal were 0 for all. Hypothesis test results can be found in Appendix F: Hypothesis tests results.

Build surface orientation at 90° was studied by Kniekamp [46] and concluded that by decreasing laser power, less dimensional error could be obtained for overhanged parts and accuracy of small cross section parts can be improved. As shows Figure 13 for 90° orientation, microneedles had a downskin layer configuration that increase the over burning, increase the dross formation and sticky powders effects (Figure 45). Those effects are produced by full melting of powder in overheated zones [30]. Considering that the absorbed input energy was bigger at the time laser irradiated the powder supported zone compared to the solid supported zone as studied [62]. The reduction of the power in downskin layers (Parameter B) was successful to improve height accuracy in this orientation.

Implementation of parameter B produced a reduction in energy density.

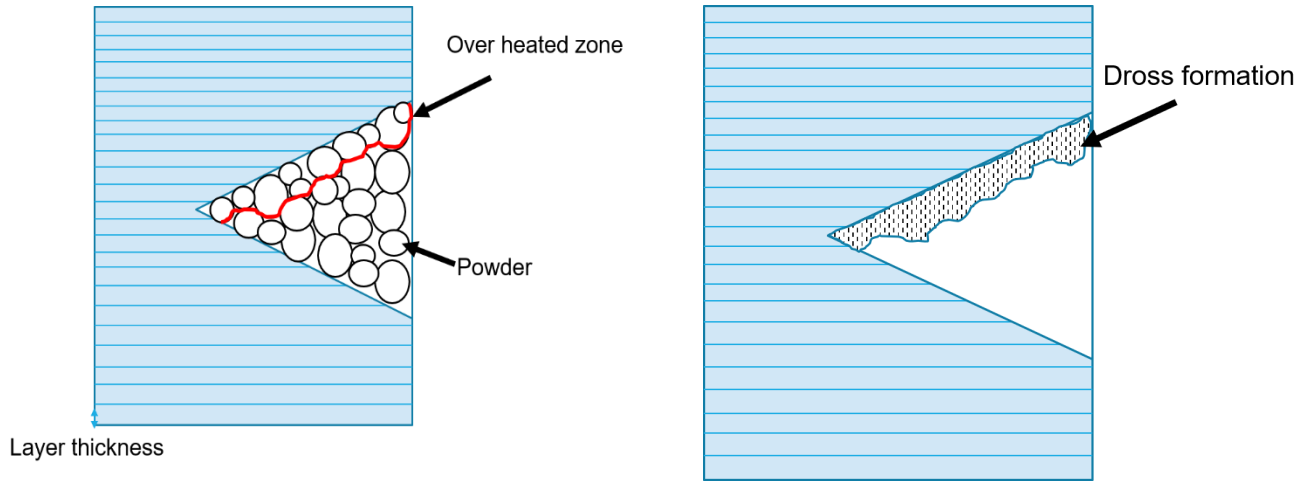


Figure 45. Dross formation effect at 90° build surface orientation

4.3 Results for Microneedle insert measurements

Table 11 shows results obtained with a Mitutoyo Vernier caliper as mentioned in Section 4.1. Thermal stress is bigger in the z planes compared to x and y plane. Results confirmed that the thickness represents the z axis value having the biggest relative error of 2.15%. Envision Tec inserts had the greatest thickness dimensional accuracy. However, for SLM inserts at 0° orientation, the lower value possibly affected the injection process molding. On the other hand, at 45° orientation, this value is bigger than nominal. Width and length values were very close to the nominal design.

Runner and gates measurements in Table 12 shows low relative error, orientation seems not to influence in this design parameters output.

Table 11. Dimensional measurement for microneedle inserts

Technology/ Orientation	Nominal			Nominal		Relative error [%]	Nominal		Relativ e error [%]
	Width [mm]	Width [mm]	Relative error [%]	Length [mm]	Length [mm]		Thickness [mm]	Thickness [mm]	
DLP 45 °	19.25	19.52	1.40	48.9	49.10	0.41	7	6.99	0.14
DLP 0°	19.25	19.44	0.99	48.9	49.28	0.78	7	6.85	2.14
SLM 0°	19.25	19.38	0.69	48.9	48.99	0.19	7	6.76	3.45
SLM 45°	19.25	19.38	0.66	48.9	49.13	0.47	7	7.07	1.00
SLM 90 °	19.25	19.16	0.48	48.9	48.58	0.66	7	6.94	0.81

Table 12. Runner and gate measurements for SLM

Description	Nominal Value [mm]	Measured value [mm]	Building orientation [°]	Relative error [%]
Top view Runner	2.38	2.39	0°	0.82
Top view Runner	2.38	2.47	90°	4.09
Top view Runner	2.38	2.40	45°	1.11
Lateral view Runner	2.38	2.34	0°	1.49
Lateral view Runner	2.38	2.35	90°	1.09
Lateral view Runner	2.38	2.35	45°	1.09
Gate	3.5	3.47	0°	0.72
Gate	3.5	3.44	90°	1.7
Gate	3.5	3.49	45°	0.01

4.4 Results validation

Finally, to compare the results obtained in this work with previous authors, 2 graphs Figure 46 and Figure 47 were done. Figure 46 shows in literature the tendency for triangular and conical bases had higher relative errors confirming that the idea for this technology to increase the sectional area, increases the accuracy in height value for microneedles. The lowest values of the graph were found in this investigation for hexagonal bases represented with the red diamond.

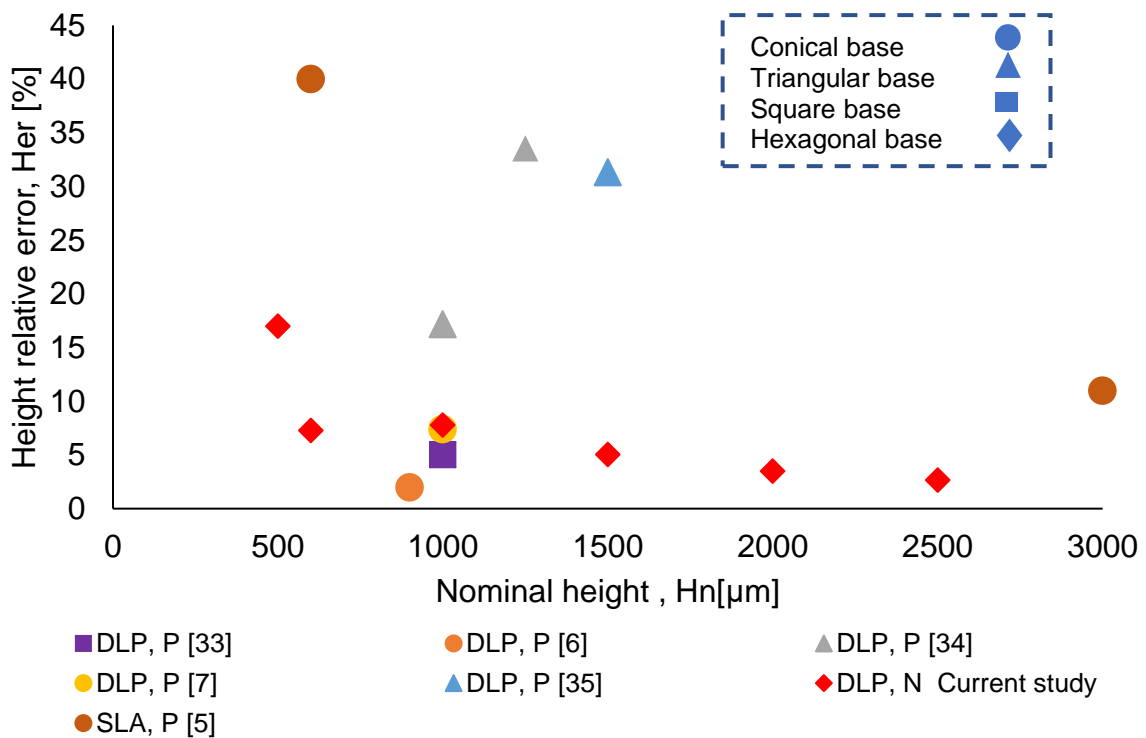


Figure 46. Comparison for this research in literature for negative microneedle construction with VAT photopolymerization technology

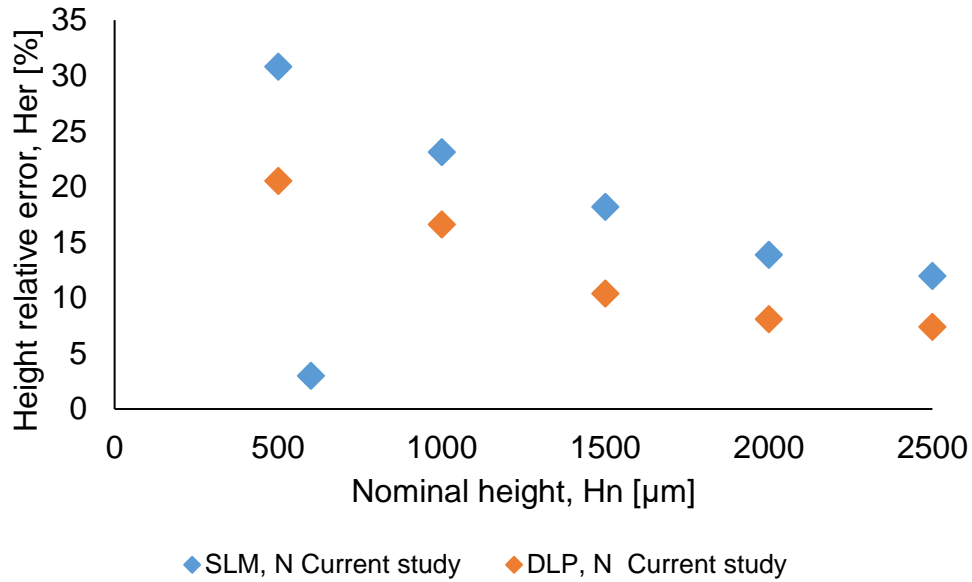


Figure 47. Comparison for this research in literature for negative microneedle construction with SLM technology

Figure 46 displays new information of capabilities for selective laser melting to produce negative microneedles using as reference data for hexagonal base designs, in a range from 500 and 2500 μm . Also, the lowest average error of 3% was obtained with the selective laser melting technology with a nominal height of 600 μm for hexagonal base applying parameter B.

Chapter 5

Conclusions

According to the objectives specified and results, the following conclusions were found:

- Hexagonal base design for microneedle cavities was the optimal because it has the biggest cross-sectional area and geometry slope angle.
- Two variables were found for technologies based on layer systems fabrication (SLM and DLP) that determine height accuracy of the microneedles cavities. The first one was the cross-sectional area and the second one was the stair stepping effect, which could be improved by increasing the angle between the geometry and the layer plane.
- For microneedles geometries fabricated with SLM, positive construction cross sectional area influenced height accuracy. In addition, tip radius results were in literature review range for skin insertion.
- Optimum building orientation for inserts manufacturing were at 45° for DLP and 0° for selective laser melting. Although, for selective laser melting at 0° orientation had the highest surface roughness value. This could improve by changing point distance, hatch distance and layer remelting.
- An increment of the surface orientation angle for the insert improved the top surface roughness average value from 24 μm at 0° to 12 μm at 90°. This can be explained due to the reduction of the energy per layer.
- Lateral surface roughness for microneedle cavities could not be obtained for this investigation because of the limited titled cavities measurement technologies.
- The mould insert at 0° and 45° had upskin configurations for microneedle compared to 90° microneedles which had downskin layer configuration. A reduction in contour and border power to 110W for

each orientation noticed an improvement in height accuracy. At 90° was the greatest improvement due to the better overhanged surface quality.

- Microneedles of 600 μm of height nominal value and a hexagonal base were manufactured in SLM with a 3% error (lowest value obtained in this work) at 0°. It was achieved by a reduction of the borders and contours laser power to 110W.

Future Work

- To modify the actual design just for hexagonal microneedle bases and modify the nominal thickness of the insert for SLM by increasing it up to 0.24 mm.
- To modify parameters for selective laser melting process to improve surface roughness. A comparison could be performed using electropolishing. Measurement of surface roughness for lateral microneedles cavities must be carried out.
- For DLP technology the ERM (enhanced resolution module) could be studied with the fabrication of microneedles cavities.
- To replicate the fabrication of different geometries for microneedle cavities in another layer system technology.
- A system for ejection of the microneedle insert from the mold cavity is necessary for the future. Although a preliminary test was done in ultrasonic injection molding process (Appendix D: Preliminary samples in ultrasonic injection process), a deeper research must be done to confirm the viability in this process. Simulations of the ultrasonic injection molding process need to be explored.

Appendix A: Abbreviations and acronyms

Table 13. Abbreviations

Description	
Microneedle	MN
PDMS	Polydimethylsiloxane
2PP	2 photon polymerizations

Table 14. Acronyms

Description	
EDM	Electric discharge machining
AM	Additive manufacturing
DLP	Digital light processing
SLA	Stereolithography
SLM	Selective laser Melting
CLIP	Continuous liquid interface production

Appendix B: QuantAM preparation

In phase 1 for the fabrication of samples for base characterization of negative and positive construction for microneedles, it was carried out using QuantAM version 4.1.0.76 of Renishaw.

The STL files made in Solid Works were imported. Pieces were put in the base plate without supports, additionally a build surface orientation of 0° was fixed as shows Figure 48. One millimeter was added to the nominal original thickness, in order to be cut in an EDM wire cut machine.

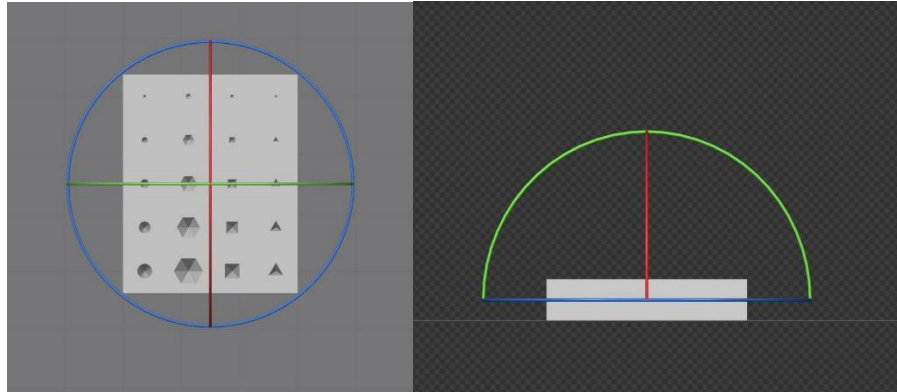


Figure 48. Build surface orientation for positive and negative microneedles

Figure 49 shows the distribution of negative and positive samples in the base plate each one had a separation of 5 mm in the X and Y axis.

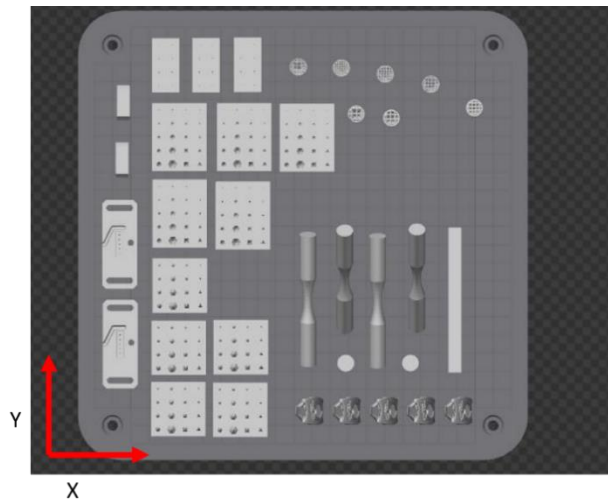


Figure 49. Distribution of test pieces in the base plate

In phase 2 for the fabrication of the microneedle insert with different build surface orientation, it was carried out using QuantAM version 5.0.0.135 of Renishaw. After the STL importation file as previous section, for microneedle inserts with build surface orientations at 0° Figure 50 and 90° Figure 51, 1 mm was added to be removed by an EDM wire cut machine. For this configuration, supports were not required.

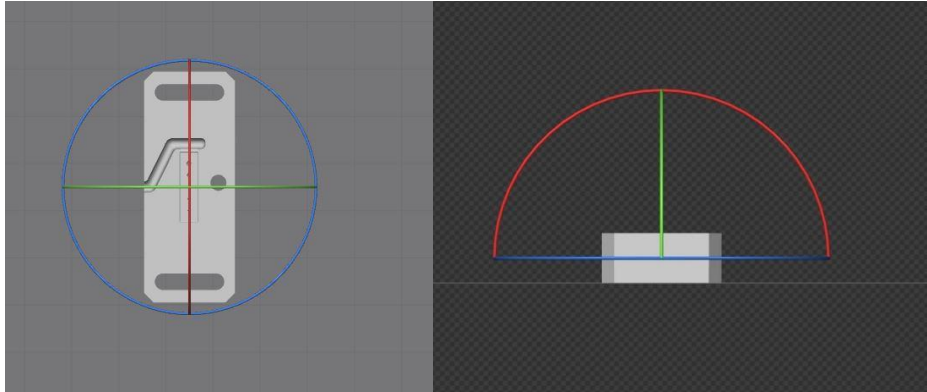


Figure 50. 0° build surface orientation for microneedle insert fabrication

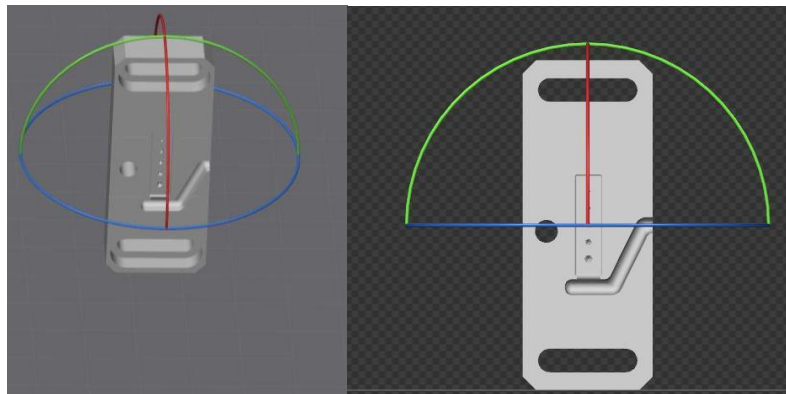


Figure 51. 90° of build surface orientation for microneedle insert fabrication

To fabricate the build surface orientation at 45° a different arrangement was done. Firstly, it was oriented 45° respect to the base plate, then an offset of 4mm in the z-axis was inserted to place supports see Figure 52.

The supports were custom, having a cross section, diameter of 0.7 mm and cover diameter 0.3 mm as shows Figure 53. Finally, distribution in the base platform is shown in Figure 54.

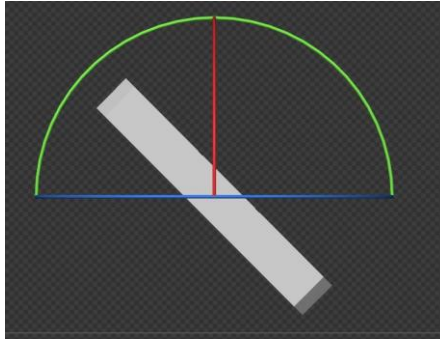


Figure 52. 45° build surface orientation with offset

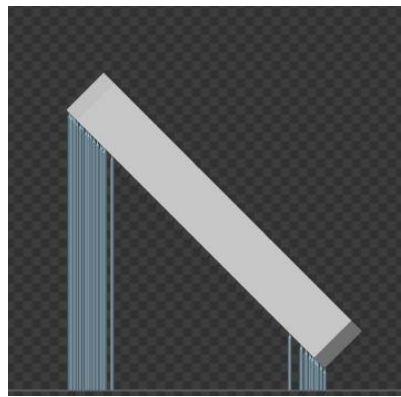


Figure 53. Microneedle insert at 45° build surface orientation with supports

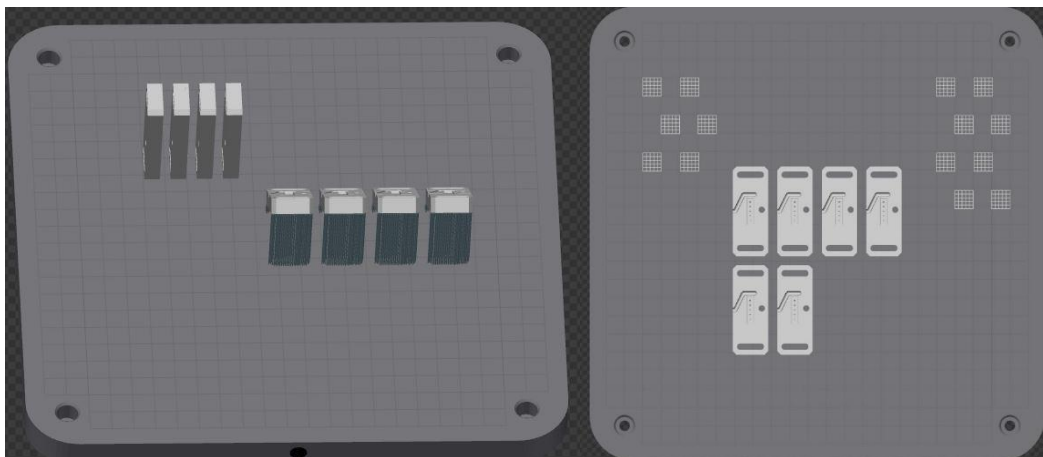


Figure 54. Distribution in base plate for 0°, 45° and 90° build surface orientations

Appendix C: Preliminary electropolishing studies

This process was carried out in the equipment Esma Inc model E782EP which is an electropolishing system where metal is being removed from the workpiece by the passage of direct electric current while the piece is submerged in a solution provided by Esma SS electropolish E972. Figure 55 is a schematic illustration of the process, the workpiece which functions as anode is connected to the positive terminal in contrast the cathode, which is connected to the positive terminal, both terminal are in a solution where complete the circuit. The following sequence of steps were carried out in the process.

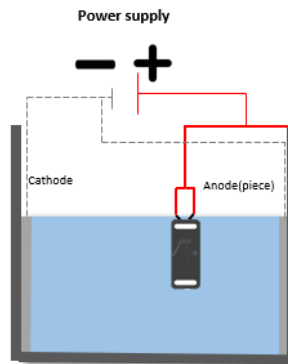


Figure 55. Electropolishing diagram

Table 15. Electropolishing process parameters

Parameter	Value
Power	30%
Voltage	12 V
Time	440 S
Temperature	60°c

1. A precleaning of pieces was carried out initially in distilled water
2. Electropolishing of Microneedle inserts was carried out in the tank 1 of the equipment with the parameters precise in Table 15. In this step, it was necessary to heat the solution before being immersed in the electropolishing kit to reach faster the temperature for electropolishing.
3. After the electropolishing, inserts were immersed in 100 ml of a mixture of 20% volume of acid nitric with a temperature of 60 °C for 4 minutes.
4. Microneedle inserts were immersed in 200 ml of saturated bicarbonate for 1 minute.
5. Finally, Inserts were immersed in distilled water for 2 minutes.

Figure 56 displays results for the electropolishing process in the microneedle insert.

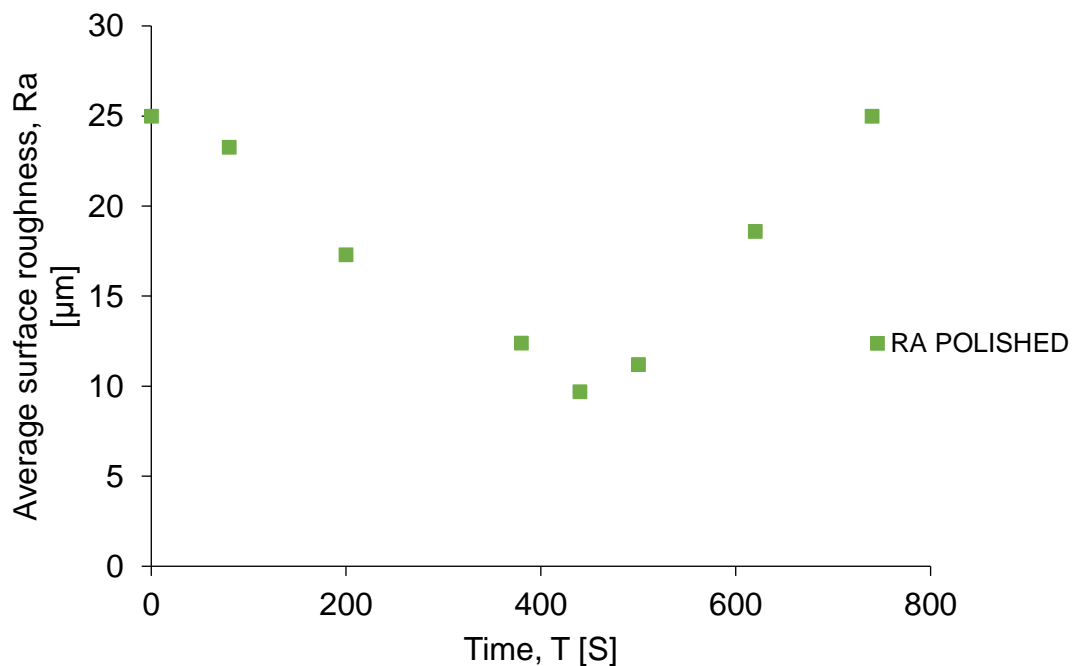


Figure 56. Electropolishing results for insert at 0° build surface orientation

Appendix D: Preliminary samples in ultrasonic injection process

Sonorous 1G ultrasonic micro molding machine developed by Ultrason SL equipment was used to validate the inserts, process parameters used in the experimentation can be found in Table 16.

Table 16. Process parameter for UIM samples

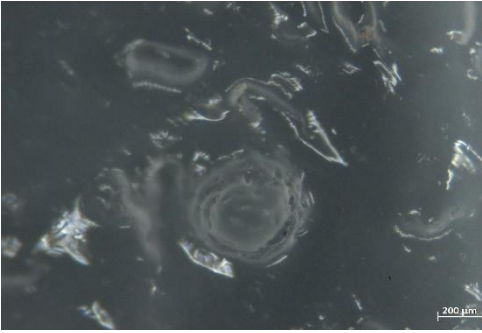

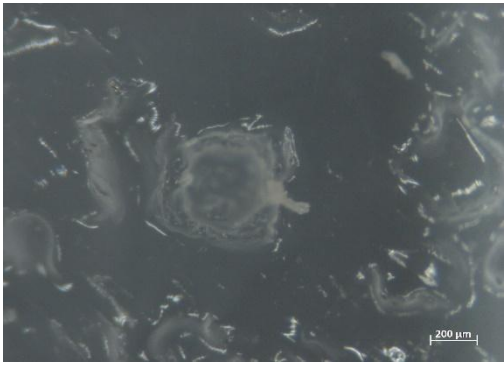
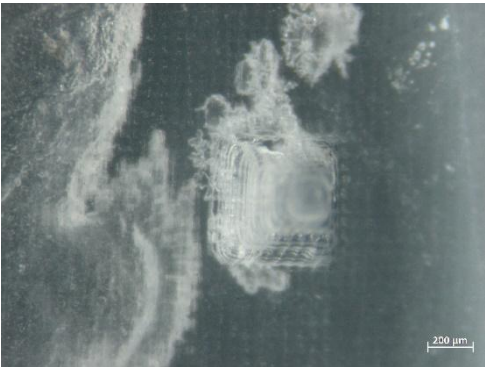
Amplitude	1 %
Force	3000 N
Plunger velocity	5.50 mm/s
Ultrasonic time	4.73 s
Cooling time	5 s

Table 17 shows the top view images for microneedles obtained from both additive manufacturing techniques fabricated in 0° orientation, geometric figures are more consistent in microneedles injected in the DLP insert this is due to the dimensional accuracy in DLP was greater than for SLM. Demolding process was easier in DLP insert this can be explained because surface roughness specially in sidewall influences in an increment of the interaction of the polymer and the mold and finally the demolding force [63], for DLP inserts a top surface roughness is of 3.5 μm however for SLM inserts after the electropolishing process had values of 9 μm. The presence of cavities in the SLM insert leads to the filtration of the molten polymer in undesirable areas as is shown in Figure 57, also it was observed that the SLM inserts had a lower height than insert cavity therefore a thin layer of polymer was formed in the base of the microneedle insert, so there is necessary to increase

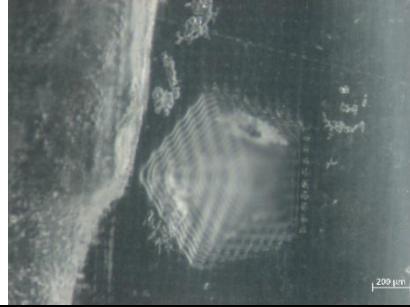
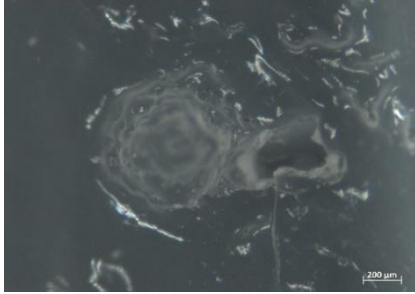
the height value parameter. Melt fracture was presented in the microneedles with DLP insert, this can be explained because in the process more volume of the polymer was injected.

100% of filling was obtained in the insert manufactured with DLP as the simulation in phase 2 predicted however for the SLM insert the triangular base was not produced, this can be explained because the flow layer is too narrowed in the SLM insert that require high injection pressures to fill the cavity the frozen layer , also as was described in simulations for triangular base is greater the drop pressure.

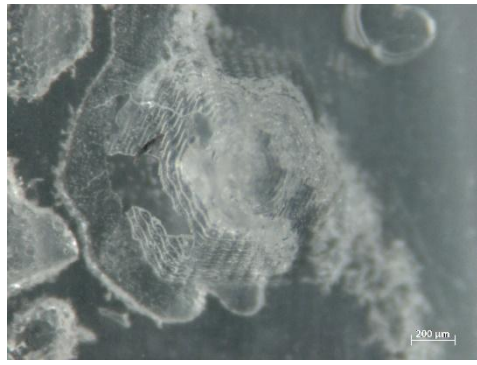
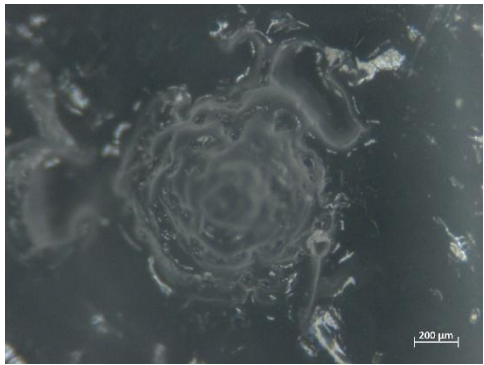
Table 17. Top view for injected microneedles

Microneedles injected samples	Microneedles injected samples
SLM	DLP
Conical	
	
Square	
	

Pentagonal



Hexagonal



Triangular

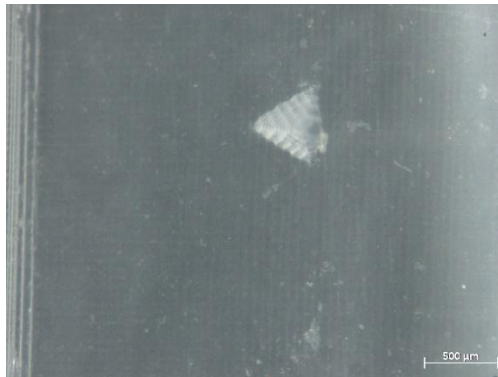




Figure 57. Ultrasonic injected Microneedle pieces. From left to right SLM insert, SLM insert and DLP insert

Figure 58 shows results for final injected Microneedles, despite of mentioned in phase for DLP process the hexagonal base did not reach the maximum output value, pentagonal base had the maximum with an average of 529.5 μm , considering this average value a dimensional error of 18% can be presented which is lower than reported in literature of 30% shorter heights. The hexagonal microneedle for the DLP insert could have had a truncation by an air trap in the tip of the microneedle so that stop the flow, also this is shown because a highest tip radius was obtained in comparison with others geometries. Gulcur et al. [25] in their research had a maximum height of 480 μm with a nominal value of 600 μm , also in another research the same author reported a height of 510 μm [49] those value are lower than obtained in the present research. DLP inserts had a better accuracy in the final microneedle than for SLM.

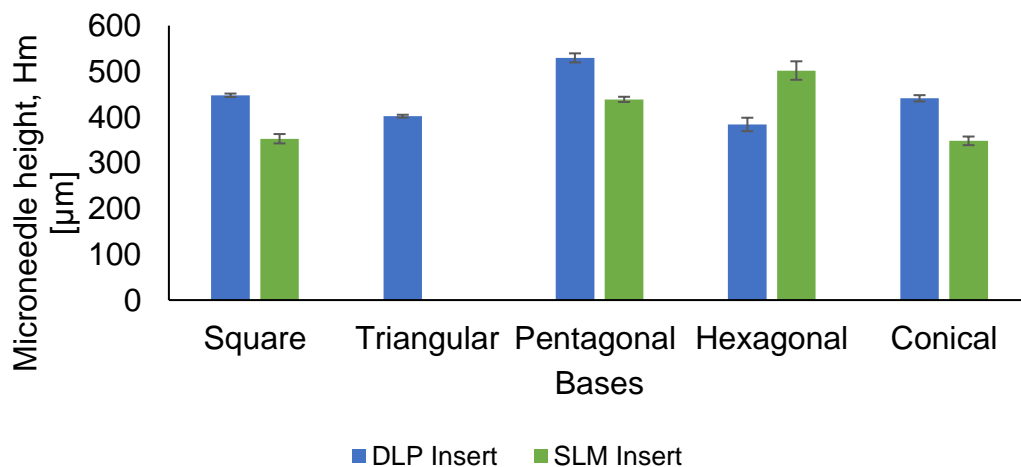


Figure 58. Height results for Microneedles in ultrasonic injection molding process

Figure 59 show results for side variable the best base was the conical and hexagonal, good values were obtained for SLM and DLP inserts, the highest average value was for conical base with 569.8 μm .

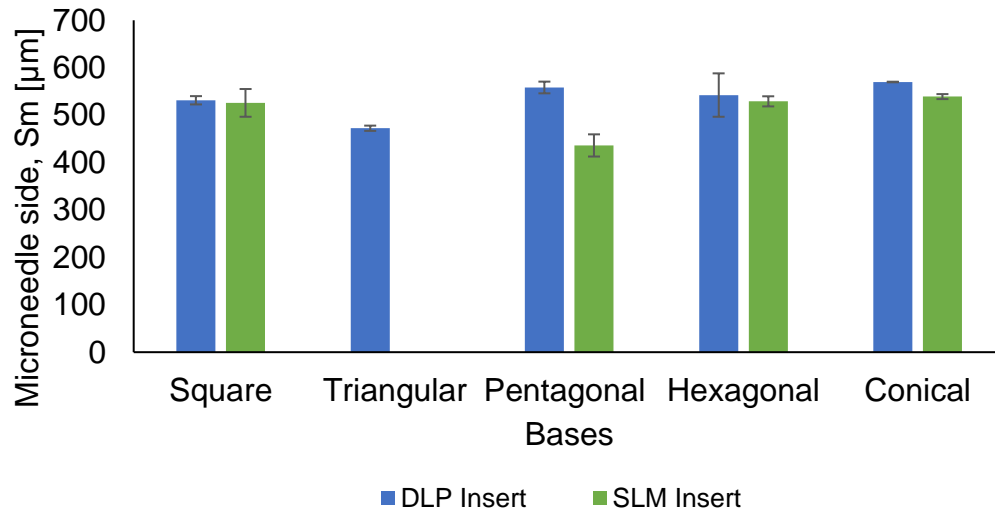


Figure 59. Side results for Microneedles in ultrasonic injection molding process

Figure 60 shows results for tip radius microneedle microneedles injected in the DLP insert , it had a closer value with literature around 40-160 [33] , the minimum tip radius was 49 μm obtained with the insert of DLP technology and the maximum of 151 μm obtained with the insert of the selective laser melting process. However, for a successful insertion into the skin (2.5 – 50 μm) values for SLM are bigger.

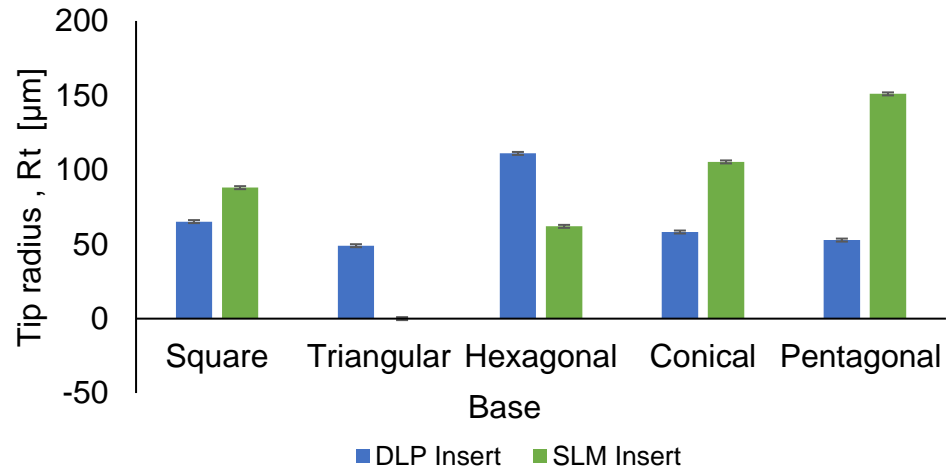


Figure 60. Tip Radius for Microneedles with ultrasonic injection Molding

Appendix E: Relative error graphs

The following equation was used to calculate the relative error for the

$$E_r = \left(\frac{\text{Nominal value} - \text{Measured value}}{\text{Nominal value}} \right) * 100$$

- **Selective laser melting**

Height variable errors for this technology in negative microneedles construction are resumed in Figure 61. In contrast for positive construction in Figure 62. Negative errors percentages mean higher results than the nominal.

Figure 63 and Figure 64 shows side variables for negative and positive construction, respectively.

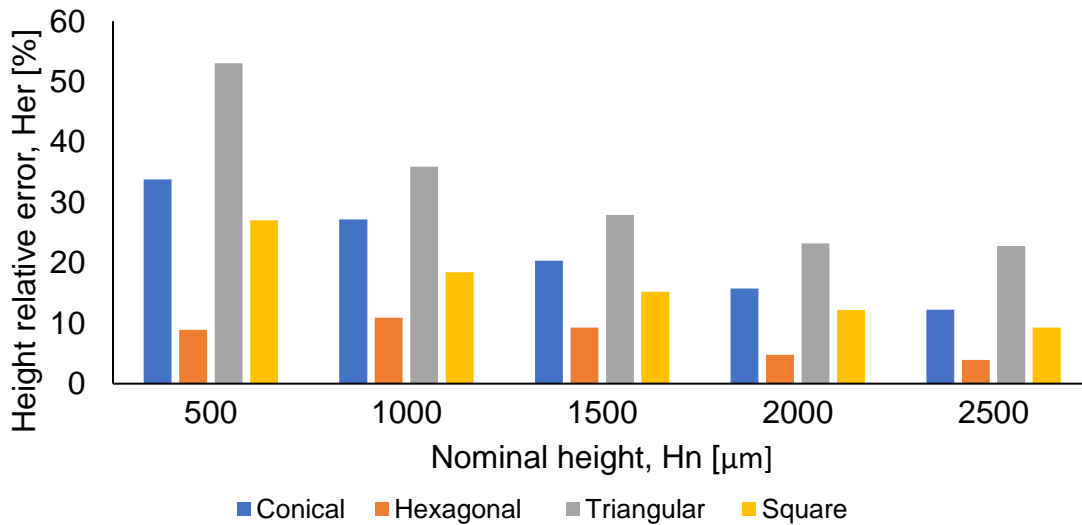


Figure 61. Height relative error for negative construction in SLM

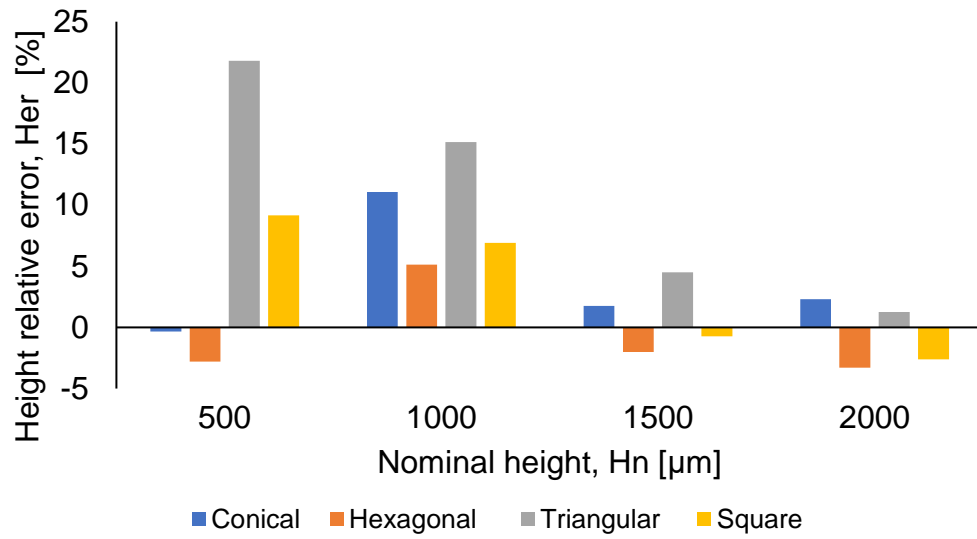


Figure 62. Height relative error for positive construction in SLM

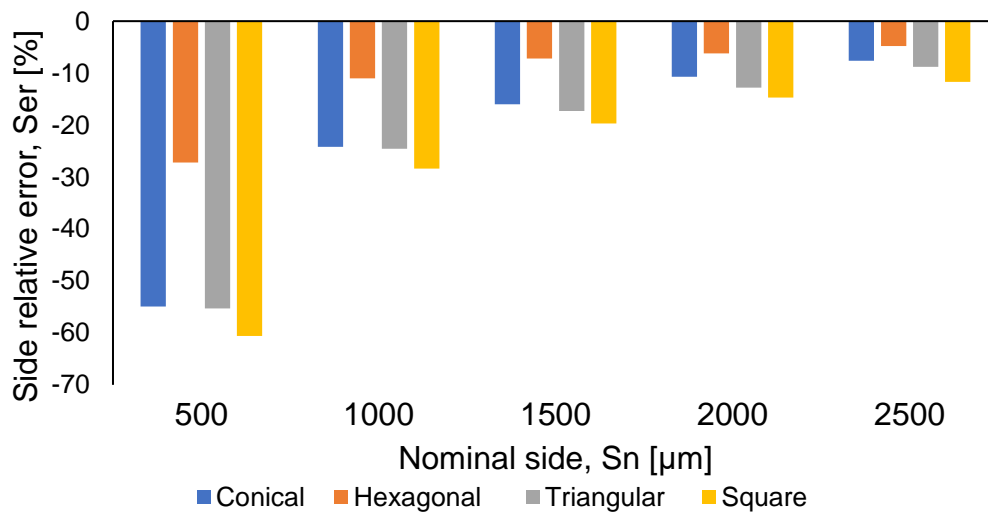


Figure 63. Side relative error for negative construction in SLM

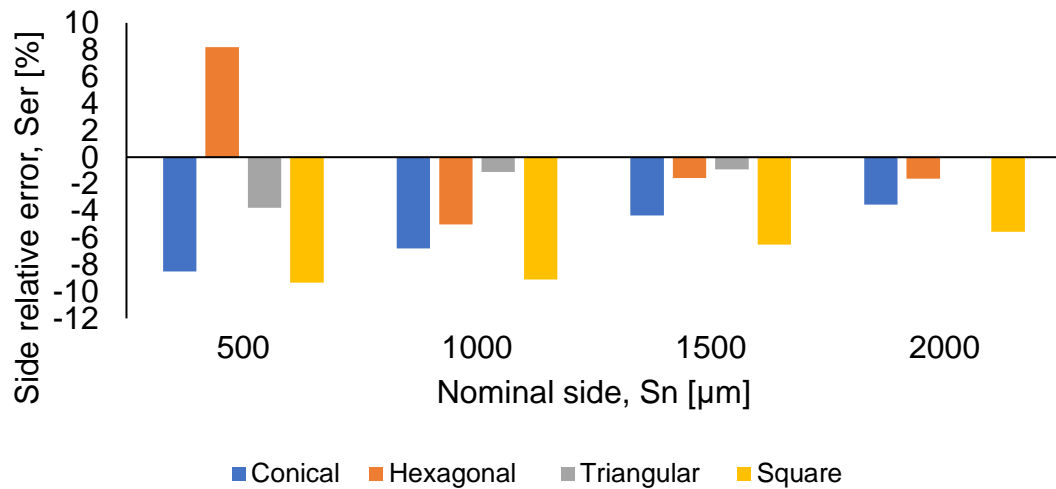


Figure 64. Side relative error for positive construction in SLM

- **Digital light processing.**

Height variable errors for this technology in negative microneedles construction are resumed in Figure 65.

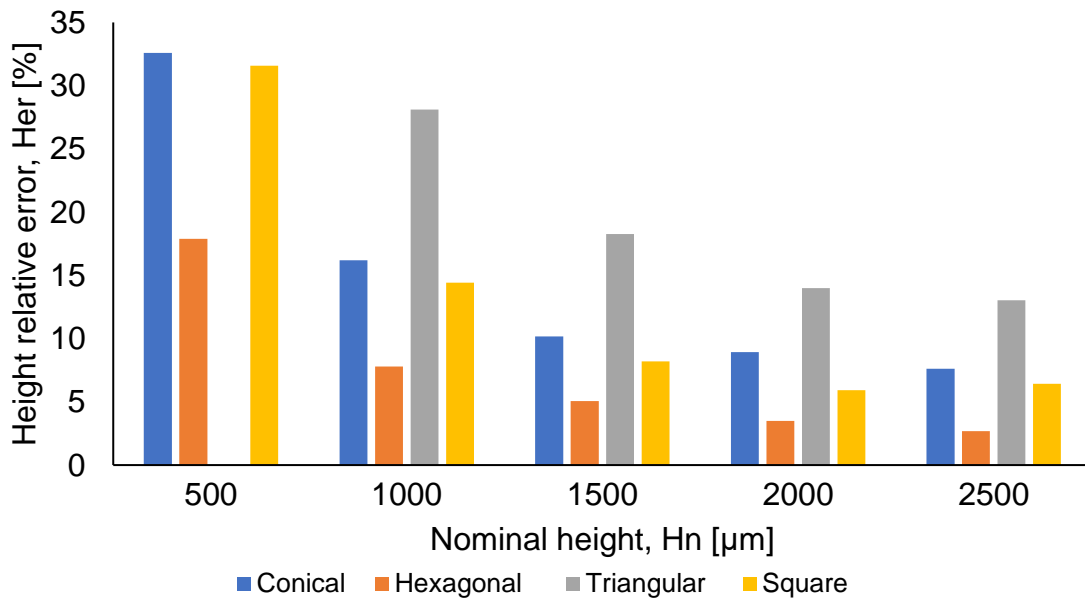


Figure 65. Height relative error for negative construction in DLP

Figure 66 shows side variables for negative construction.

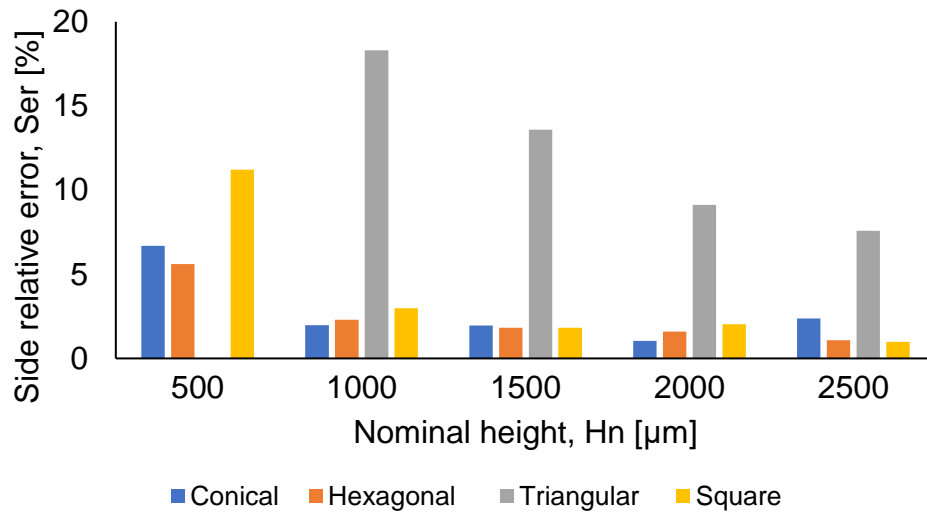


Figure 66. Side relative error for negative construction in DLP

Appendix F: Hypothesis tests results

This section includes results for hypothesis test to confirm mean of parameter B is greater than parameter A at different orientations for SLM results, with a significance level of 0.05.

$$\begin{aligned}\mu_1 &= \text{mean of parameter A} \\ \mu_2 &= \text{mean of parameter B}\end{aligned}$$

- Selective laser melting at 0° orientation

✓ Triangular base

Table 18. Hypothesis test for triangular base at 0° orientation

Null hypothesis	$H_0: \mu_1 - \mu_2 = 0$		
Alternative hypothesis	$H_1: \mu_1 - \mu_2 < 0$		
T-Value	DF	P-Value	
-3.59	6	0.006	

At 0° orientation, for triangular base parameter B improved height accuracy

✓ Conical base

Table 19. Hypothesis test for conical base at 0° orientation

Null hypothesis	$H_0: \mu_1 - \mu_2 = 0$		
Alternative hypothesis	$H_1: \mu_1 - \mu_2 < 0$		
T-Value	DF	P-Value	
-0.80	6	0.226	

At 0° orientation, for conical base parameter B did not improve height accuracy.

✓ Square base

Table 20. Hypothesis test for square base at 0° orientation

Null hypothesis	$H_0: \mu_1 - \mu_2 = 0$		
Alternative hypothesis	$H_1: \mu_1 - \mu_2 < 0$		
T-Value	DF	P-Value	
1.07	7	0.840	

At 0° orientation, for square base parameter B did not improve height accuracy.

✓ Pentagonal base

Table 21. Hypothesis test for pentagonal base at 0° orientation

Null hypothesis	$H_0: \mu_1 - \mu_2 = 0$		
Alternative hypothesis	$H_1: \mu_1 - \mu_2 < 0$		
T-Value	DF	P-Value	
-0.80	5	0.229	

At 0° orientation, for pentagonal base parameter B did not improve height accuracy.

✓ Hexagonal base

Table 22. Hypothesis test for hexagonal base at 0° orientation

Null hypothesis	$H_0: \mu_1 - \mu_2 = 0$		
Alternative hypothesis	$H_1: \mu_1 - \mu_2 < 0$		
T-Value	DF	P-Value	
-9.44	13	0.000	

At 0° orientation, for hexagonal base parameter B improved height accuracy.

- Selective laser melting at 45° orientation.

✓ Triangular base

Table 23. Hypothesis test for triangular base at 45° orientation

Null hypothesis			$H_0: \mu_1 - \mu_2 = 0$
Alternative hypothesis			$H_1: \mu_1 - \mu_2 < 0$
T-Value	DF	P-Value	
5.07	11	1.000	

At 45° orientation, for triangular base parameter B did not improve height accuracy.

✓ Conical base

Table 24. Hypothesis test for conical base at 45° orientation

Null hypothesis			$H_0: \mu_1 - \mu_2 = 0$
Alternative hypothesis			$H_1: \mu_1 - \mu_2 < 0$
T-Value	DF	P-Value	
-2.69	11	0.010	

At 45° orientation, for conical base parameter B improved height accuracy.

✓ Square base

Table 25. Hypothesis test for square base at 45° orientation

Null hypothesis			$H_0: \mu_1 - \mu_2 = 0$
Alternative hypothesis			$H_1: \mu_1 - \mu_2 < 0$
T-Value	DF	P-Value	

-1.65	13	0.062
-------	----	-------

At 45° orientation, for square base parameter B did not improve height accuracy

✓ Pentagonal base

Table 26. Hypothesis test for pentagonal base at 45° orientation

Null hypothesis	$H_0: \eta_1 - \eta_2 = 0$	
Alternative hypothesis	$H_1: \eta_1 - \eta_2 < 0$	
Method	W-Value	P-Value
Not adjusted for ties	36.00	0.000
Adjusted for ties	36.00	0.000

At 45° orientation, for pentagonal base parameter B improved height accuracy.

✓ Hexagonal base

Table 27. Hypothesis test for hexagonal base at 45° orientation

Null hypothesis	$H_0: \mu_1 - \mu_2 = 0$	
Alternative hypothesis	$H_1: \mu_1 - \mu_2 < 0$	
T-Value	DF	P-Value
-0.54	13	0.298

At 45° orientation, for hexagonal base parameter B did not improve height accuracy.

- Selective laser melting at 90° orientation.

✓ Triangular base

Table 28. Hypothesis test for triangular base at 90° orientation

Null hypothesis	$H_0: \mu_1 - \mu_2 = 0$	
Alternative hypothesis	$H_1: \mu_1 - \mu_2 < 0$	
T-Value	DF	P-Value

-6.86	9	0.000
-------	---	-------

At 90° orientation, for triangular base parameter B improved height accuracy.

✓ Conical base

Table 29. Hypothesis test for conical base at 90° orientation

Null hypothesis	$H_0: \eta_1 - \eta_2 = 0$	
Alternative hypothesis	$H_1: \eta_1 - \eta_2 < 0$	
W-Value	p-value	
68.00	0.521	

At 90° orientation, for conical base parameter B did not improve height accuracy.

✓ Square base

Table 30. Hypothesis test for square base at 90° orientation

Null hypothesis	$H_0: \mu_1 - \mu_2 = 0$	
Alternative hypothesis	$H_1: \mu_1 - \mu_2 < 0$	
T-Value	DF	P-Value
-5.87	12	0.000

At 90° orientation, for square base, parameter B improved height accuracy.

✓ Pentagonal base

Table 31. Hypothesis test for pentagonal base at 90° orientation

Null hypothesis	$H_0: \mu_1 - \mu_2 = 0$	
Alternative hypothesis	$H_1: \mu_1 - \mu_2 < 0$	
T-Value	DF	P-Value
-6.73	10	0.000

At 90° orientation, for pentagonal base, parameter B improved height accuracy.

✓ Hexagonal base

Table 32. Hypothesis test for hexagonal base at 90° orientation

Null hypothesis	$H_0: \mu_1 - \mu_2 = 0$	
Alternative hypothesis	$H_1: \mu_1 - \mu_2 < 0$	
T-Value	DF	P-Value
-5.08	12	0.000

At 90° orientation, for hexagonal base, parameter B improved height accuracy

Bibliography

- [1] F. business Insight, "3D Printing Medical Devices Market Sizes, Share and Global Trends By Products. products,orthopedic Products," 2018.
- [2] F. business Insight, "Drug Delivery Devices Market Size, Share & Industry Analisis, By Route Of Administration,By Type, By distribution Channel, and regional forecast," 2018.
- [3] H. Juster, B. van der Aar, and H. de Brouwer, "A review on microfabrication of thermoplastic polymer-based microneedle arrays," *Polym. Eng. Sci.*, vol. 59, no. 5, pp. 877–890, 2019.
- [4] J. C. Vasco, I. S. Ferreira, and A. S. Pouzada, "Evaluation of the performance of micromoulding blocks using micromanufacturing technologies," *Adv. Prod. Eng. Manag.*, vol. 8, no. 2, pp. 78–87, 2013.
- [5] K. J. Krieger, N. Bertollo, M. Dangol, J. T. Sheridan, M. M. Lowery, and E. D. O’Cearbhaill, "Simple and customizable method for fabrication of high-aspect ratio microneedle molds using low-cost 3D printing," *Microsystems Nanoeng.*, vol. 5, no. 1, 2019.
- [6] F. Lacan, S. A. Coulman, A. Hotston, P. Petkov, and J. C. Birchall, "Prototyping Parts with Micro Scale Features Using Additive Manufacturing: Using Microneedles as a Case Study," pp. 109–113, 2013.
- [7] R. D. Boehm, P. R. Miller, S. L. Hayes, N. A. Monteiro-Riviere, and R. J. Narayan, "Modification of microneedles using inkjet printing," *AIP Adv.*, vol. 1, no. 2, 2011.
- [8] S. N. Economidou, D. A. Lamprou, and D. Douroumis, "3D printing applications for transdermal drug delivery," *Int. J. Pharm.*, vol. 544, no. 2, pp. 415–424, 2018.
- [9] E. Yasa and J. Kruth, "Application of Laser Re-Melting on Selective Laser Melting Parts," *Adv. Prod. Eng. ...*, vol. 6, no. 4, pp. 259–270, 2011.
- [10] M. Gieseke *et al.*, "Additive manufacturing of drug delivery systems," *Biomed. Tech.*, vol. 57, no. SUPPL. 1 TRACK-S, pp. 398–401, 2012.
- [11] J. C. Vasco and A. S. Pouzada, "A study on microinjection moulding using moulding blocks by additive micromanufacturing," *Int. J. Adv. Manuf. Technol.*,

vol. 69, no. 9–12, pp. 2293–2299, 2013.

- [12] S. Indermun *et al.*, “Current advances in the fabrication of microneedles for transdermal delivery,” *J. Control. Release*, vol. 185, no. 1, pp. 130–138, 2014.
- [13] E. Larrañeta, R. E. M. Lutton, A. D. Woolfson, and R. F. Donnelly, “Microneedle arrays as transdermal and intradermal drug delivery systems: Materials science, manufacture and commercial development,” *Mater. Sci. Eng. R Reports*, vol. 104, pp. 1–32, 2016.
- [14] A. R. Johnson *et al.*, “Single-step fabrication of computationally designed microneedles by continuous liquid interface production,” *PLoS One*, vol. 11, no. 9, pp. 1–17, 2016.
- [15] M. Ogundele and H. Okafor, “Transdermal Drug Delivery: Microneedles, Their Fabrication and Current Trends in Delivery Methods,” *J. Pharm. Res. Int.*, vol. 18, no. 5, pp. 1–14, 2017.
- [16] Z. C. L. L. R. L. L. W. Jiang*, “Additive Manufacturing of Honeybee-Inspired Microneedle for Easy Skin Insertion and Difficult Removal,” *Chem. Soc.*, vol. 10, no. 35, 2018.
- [17] E. García-López, H. R. Siller, and C. A. Rodríguez, “Study of the fabrication of AISI 316L microneedle arrays,” *Procedia Manuf.*, vol. 26, pp. 117–124, 2018.
- [18] K. J. NAIR, “PhD thesis, Micro-Injection Moulded Microneedles For Drug Delivery,” *PhD thesis Univ. Bradford*, 2014.
- [19] S. K. Choudhary and R. S. Jadoun, “Current Advanced Research Development of Electric Discharge Machining (EDM): A Review,” *Int. J. Res. Advent Technol.*, vol. 2, no. 3, pp. 2321–9637, 2014.
- [20] H. Becker and U. Heim, “Hot embossing as a method for the fabrication of polymer high aspect ratio structures,” *Sensors Actuators, A Phys.*, vol. 83, no. 1, pp. 130–135, 2000.
- [21] Q. L. Wang, D. D. Zhu, Y. Chen, and X. D. Guo, “A fabrication method of microneedle molds with controlled microstructures,” *Mater. Sci. Eng. C*, vol. 65, pp. 135–142, 2016.
- [22] C. A. Griffiths, S. S. Dimov, E. B. Brousseau, and R. T. Hoyle, “The effects of tool surface quality in micro-injection moulding,” *J. Mater. Process. Technol.*,

vol. 189, no. 1–3, pp. 418–427, 2007.

- [23] T. Dorf, “CONTRIBUTION TO ULTRASONIC MICRO-MOULDING PROCESS OF HIGH PERFORMANCE POLYMERS,” 2019.
- [24] U. Heredia-Rivera, I. Ferrer, and E. Vázquez, “Ultrasonic molding technology: Recent advances and potential applications in the medical industry,” *Polymers (Basel)*, vol. 11, no. 4, pp. 1–25, 2019.
- [25] M. Gulcur, B. R. Whiteside, K. Nair, M. Babenko, and P. D. Coates, “Ultrasonic injection moulding of polypropylene and thermal visualisation of the process using a bespoke injection mould tool,” *Eur. Soc. Precis. Eng. Nanotechnology, Conf. Proc. - 18th Int. Conf. Exhib. EUSPEN 2018*, no. June, pp. 243–244, 2018.
- [26] C. P. P. Pere *et al.*, “3D printed microneedles for insulin skin delivery,” *Int. J. Pharm.*, vol. 544, no. 2, pp. 425–432, 2018.
- [27] S. L. M. 1 and P. A. F. 1 Albert E. Patterson 1, 2,* , “Overhanging Features and the SLM/DMLS Residual Stresses Problem: Review and Future Research Need.” .
- [28] I. O. for Standardization, *ISO/ASTM 52900:2015. Additive manufacturing–General principles–terminology. Title.* 2015.
- [29] C. Groth, N. D. Kravitz, P. E. Jones, J. W. Graham, and W. R. Redmond, “Three-dimensional printing technology,” *J. Clin. Orthod.*, vol. 48, no. 8, pp. 475–485, 2014.
- [30] A. Charles, A. Elkaseer, L. Thijs, V. Hagenmeyer, and S. Scholz, “Effect of process parameters on the generated surface roughness of down-facing surfaces in selective laser melting,” *Appl. Sci.*, vol. 9, no. 6, pp. 1–13, 2019.
- [31] S. D. Gittard, A. Nguyen, K. Obata, A. Koroleva, R. J. Narayan, and B. N. Chichkov, “Fabrication of microscale medical devices by two-photon polymerization with multiple foci via a spatial light modulator,” *Biomed. Opt. Express*, vol. 2, no. 11, p. 3167, 2011.
- [32] C. Farias *et al.*, “Three-dimensional (3D) printed microneedles for microencapsulated cell extrusion,” *Bioengineering*, vol. 5, no. 3, 2018.
- [33] A. R. Johnson and A. T. Procopio, “Low cost additive manufacturing of

- microneedle masters,” *3D Print. Med.*, vol. 5, no. 1, 2019.
- [34] S. D. Gittard *et al.*, “Deposition of antimicrobial coatings on microstereolithography-fabricated microneedles,” *Jom*, vol. 63, no. 6, pp. 59–68, 2011.
- [35] P. R. Miller *et al.*, “Integrated carbon fiber electrodes within hollow polymer microneedles for transdermal electrochemical sensing,” *Biomicrofluidics*, vol. 5, no. 1, pp. 1–14, 2011.
- [36] 4 Ryan D Boehm¹, Philip R Miller¹, Ritika Singh¹, Akash Shah², Shane Stafslie³, Justin Daniels³ and Roger J Narayan¹, “Indirect rapid prototyping of antibacterial acid anhydride copolymer microneedles,” *IOP Sci.*, 2012.
- [37] Z. Ali, E. B. Türeyen, Y. Karpat, and M. Çakmakci, “Fabrication of Polymer Micro Needles for Transdermal Drug Delivery System Using DLP Based Projection Stereo-lithography,” *Procedia CIRP*, vol. 42, no. Isem Xviii, pp. 87–90, 2016.
- [38] Renishaw, “SS 316L-0407 powder for additive manufacturing,” vol. 2001, no. Iso 97, pp. 0–1, 2001.
- [39] EnvisionTEC GmbH, “Htm 140 V2 Technical Datasheet,” p. 3350, 2018.
- [40] Renishaw, “AM 400 additive manufacturing system Flexible metal additive manufacturing (AM),” p. 2, 2019.
- [41] E. Ramirez-Cedillo, J. A. Sandoval-Robles, L. Ruiz-Huerta, A. Caballero-Ruiz, C. A. Rodriguez, and H. R. Siller, “Process planning guidelines in selective laser melting for the manufacturing of stainless steel parts,” *Procedia Manuf.*, vol. 26, no. September, pp. 973–982, 2018.
- [42] S. Clijsters, T. Craeghs, M. Moesen, and J.-P. Kruth, “Optimization of thin wall structures in SLM,” *Direct Digit. Manuf. Conf.*, 2012.
- [43] W. Shi, P. Wang, Y. Liu, and G. Han, “Experiment of process strategy of selective laser melting forming metal nonhorizontal overhanging structure,” *Metals (Basel)*, vol. 9, no. 4, 2019.
- [44] Ahmed, Majeed, Atta, and Guozhu, “Dimensional Quality and Distortion Analysis of Thin-Walled Alloy Parts of AlSi10Mg Manufactured by Selective Laser Melting,” *J. Manuf. Mater. Process.*, vol. 3, no. 2, p. 51, 2019.

- [45] N. C. Sabina L. Campanelli and A. A. and A. D. Ludovico, "Capabilities and Performances of the Selective Laser Melting Process," *Intech*, 2010.
- [46] M. Kniepkamp, J. Fischer, and E. Abele, "Dimensional accuracy of small parts manufactured by micro selective laser melting," *Proc. 27th Annu. Int. Solid Free. Fabr. 2016*, pp. 1530–1537, 2016.
- [47] L. Zhang, S. Zhang, H. Zhu, Z. Hu, G. Wang, and X. Zeng, "Horizontal dimensional accuracy prediction of selective laser melting," *Mater. Des.*, vol. 160, pp. 9–20, 2018.
- [48] B. Song *et al.*, "Differences in microstructure and properties between selective laser melting and traditional manufacturing for fabrication of metal parts: A review," *Front. Mech. Eng.*, vol. 10, no. 2, pp. 111–125, 2015.
- [49] M. Gulcur, B. Whiteside, P. Fook, K. Rickens, and O. Riemer, "Process and product fingerprint concept for microinjection moulding of thermoplastic microneedle arrays," *Eur. Soc. Precis. Eng. Nanotechnology, Conf. Proc. - 19th Int. Conf. Exhib. EUSPEN 2019*, no. June, pp. 238–239, 2019.
- [50] K. J. Cha, T. Kim, S. J. Park, and D. S. Kim, "Simple and cost-effective fabrication of solid biodegradable polymer microneedle arrays with adjustable aspect ratio for transdermal drug delivery using acupuncture microneedles," *J. Micromechanics Microengineering*, vol. 24, no. 11, 2014.
- [51] S. N. Economidou *et al.*, "3D printed microneedle patches using stereolithography (SLA) for intradermal insulin delivery," *Mater. Sci. Eng. C*, vol. 102, no. October 2018, pp. 743–755, 2019.
- [52] P. J. Bártolo, *Stereolithography: Materials, Processes and Applications*. Portugal: Springer US, 2011.
- [53] J. Yasa, Evren. Craeghs, Tom. Kruth, "INVESTIGATION ON OCCURRENCE OF ELEVATED EDGES IN SELECTIVE LASER MELTING," *مجلة العربية*, vol. 2, no. 5, p. 255, 2009.
- [54] A. Khoshkhoo, A. L. Carrano, and D. M. Biersch, "Effect of surface slope and build orientation on surface finish and dimensional accuracy in material jetting processes," *Procedia Manuf.*, vol. 26, pp. 720–730, 2018.
- [55] E. Yasa and J. Kruth, "Application of Laser Re-Melting on Selective Laser

- Melting Parts,” *Adv. Prod. Eng. Manag.*, vol. 6, no. 4, pp. 259–270, 2011.
- [56] K. Alrbaey, D. Wimpenny, R. Tosi, W. Manning, and A. Moroz, “On optimization of surface roughness of selective laser melted stainless steel parts: A statistical study,” *J. Mater. Eng. Perform.*, vol. 23, no. 6, pp. 2139–2148, 2014.
- [57] R. Rashid *et al.*, “Effect of energy per layer on the anisotropy of selective laser melted AlSi12 aluminium alloy,” *Addit. Manuf.*, vol. 22, pp. 426–439, 2018.
- [58] J. A. Cherry, H. M. Davies, S. Mehmood, N. P. Lavery, S. G. R. Brown, and J. Sienz, “Investigation into the effect of process parameters on microstructural and physical properties of 316L stainless steel parts by selective laser melting,” *Int. J. Adv. Manuf. Technol.*, vol. 76, no. 5–8, pp. 869–879, 2014.
- [59] E. Ramirez-Cedillo *et al.*, “Process planning of L-PBF of AISI 316L for improving surface quality and relating part integrity with microstructural characteristics,” *Surf. Coatings Technol.*, vol. 396, no. May, p. 125956, 2020.
- [60] B. AlMangour, D. Grzesiak, and J. M. Yang, “Scanning strategies for texture and anisotropy tailoring during selective laser melting of TiC/316L stainless steel nanocomposites,” *J. Alloys Compd.*, vol. 728, pp. 424–435, 2017.
- [61] E. Yasa and J. P. Kruth, “Microstructural investigation of selective laser melting 316L stainless steel parts exposed to laser re-melting,” *Procedia Eng.*, vol. 19, pp. 389–395, 2011.
- [62] D. Wang, Y. Yang, Z. Yi, and X. Su, “Research on the fabricating quality optimization of the overhanging surface in SLM process,” *Int. J. Adv. Manuf. Technol.*, vol. 65, no. 9–12, pp. 1471–1484, 2013.
- [63] T. Struklec, “On the demolding of micro-structured surfaces for medical applications by,” 2011.

Curriculum

Cindy Meneses Ricaurte was born in Barranquilla, Colombia, she studied industrial engineering at Universidad del Atlántico. She was part of ANEIAP an association of industrial engineers, she was part of the directive team of the association for the university representation.

Also lead the organization of national congress. She got her bachelor's degree in 2016, while she was working in Postobón as a production analyst. After 2 years and 7 months working in the production area, she decided to move to México to study a master's degree in manufacturing systems, she was accepted in May of 2018 by the Tecnológico de Monterrey.

After being admitted, she started to work with the advanced manufacturing group with Dra. Elisa Virginia Vázquez Lepe and Dra. Erika García López.